DEVELOPMENT AND EVALUATION OF CHLOROPHYLL SYNTESISED SOLAR CELL.

Eshetu Mentesenot A.∗1, Lekeka Biniam B.†2, Tasisa Dawit M.1, and Itefa Sura Kenasa.1

Department of Advanced Materials Science, MISIS University, RUSSIA

Abstract

Currently, natural dye-based dye-sensitized solar cells (DSSCs) have drawn enormous attention owing to their numerous advantages, such as cost-effectiveness, simple production systems, and eco-friendliness. The aim of this project was to conduct combined experimental investigations on potassium iodide and starch gel electrolytes for the conversion of photoelectrochemically synthesized solar cell extracts using chlorophyll (Azadirachta indica) as a natural dye photosensitizer for application in TiO_2 based DSSCs. The optical properties and functional groups of the tin oxide-coated glass were determined using FTIR and XRD to determine the crystal size of the tin oxide. TiO_2-based DSSCs containing I^-/I_3^- as a redox mediator and graphite-carbon-based microscopic substrate slide glass as a counter electrode, and the difference between the use of gel electrolyte and liquid electrolyte on the DSSC performance. Sandwich cells were made consisting of a working electrode in the form of a conductive glass ITO deposited with TiO_2, which was sensitized by a dye of neem leaf extract; the opposite electrode in the form of a conductive glass ITO with candle smoke deposited; and the electrolyte in the middle of the two electrodes was liquid and one was gel. Both samples were irradiated with sunlight. We tested the characteristics of voltage-time and current-time in both samples as short circuit case and photo voltage evaluation on dye-synthesized solar cells, as well as investigation of the respective electrolytes. The current and voltage values for the cell were 33.33 $\mu A/mm^2$ for the potassium iodide electrolyte test and 4.66 $\mu A/mm^2$ for the starch gel electrolyte as the short-circuit case and 540 kVand180kV for the potassium iodide and starch gel, respectively. The results obtained for higher voltage and current values in samples with liquid electrolytes, but for the period of stability, the samples with gel electrolytes exhibited better performance.

Keywords: gel electrolyte; liquid electrolyte; neem leaf (Azardinchita indica) extract; TiO_2 nanoparticles.

CHAPTER ONE

1. INTRODUCTION

1.1. Background

Over billions of years, the Earth has been converting sunlight into energy via photosynthesis. Sunlight is the most abundant and sustainable source of energy. The Earth receives energy from the sun at a rate of ~1.2×10^{17} J s^{-1} [1]. This exceeded the yearly worldwide energy consumption rate of ~1.5×10^{13} J s^{-1}[1]. Therefore, it is a challenge to devise an approach for the effective capture and storage of solar energy because fossil fuels such as oil and gas will be depleted in the coming years [2]. To imitate the photosynthetic process, Grätzel developed dye-sensitized solar cells (DSSCs) based on a similar

mechanism [3]. Figure 1 shows a typical DSSC. Nevertheless, one main difference between photosynthesis of plants and DSSCs is that the energy can be stored in plants for later use, but DSSC are unable to store energy. Ever since the birth of DSSCs, they have become the spotlight of attention among scientists and researchers around the world as they are much cheaper, easier to fabricate, and more environmentally friendly when compared with conventional silicon solar cells
[4].

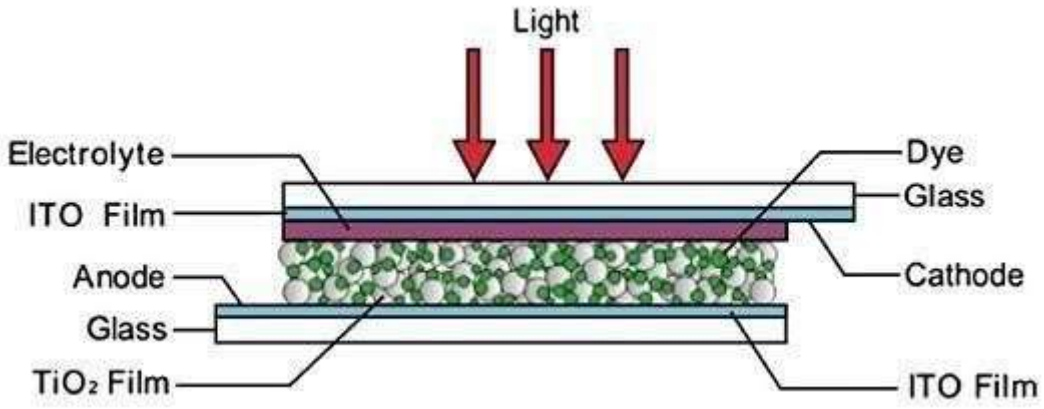

Figure 1:Structure of photosynthetic pigments-sensitized TiO2 solar cell

A DSSC is an electrochemical device that comprises a transparent-conducting oxide (TCO) glass over which is deposited a semiconductor. The semiconductor was then soaked in dye solution. An electrolyte with a reduction-oxidation (redox) mediator and a cathode are the remaining components. The fluorine-doped tin oxide (microscopic substrate)/semiconductor/dye assembly is referred to as the photoanode. Indium-doped tin oxide (ITO) and microscopic substrates are two TCOs commonly used in DSSCs. Titanium dioxide (TiO_2) is a popular semiconductor used in DSSC because it is cheap, nontoxic, and possesses a large bandgap [5]. TiO_2 was deposited on the TCO substrate in the form of a TiO_2 nanoporous particle network to increase the coverage area of the sensitizing dye. The cathode is composed of another TCO on top of which platinum is deposited. Carbon and conducting polymers can also be used as counter electrodes. If a gel polymer electrolyte is used, it is sandwiched between the photoanode and the cathode. Dyes, on the other hand, can be categorized into two groups: synthetic and natural. Ruthenium (Ru)-based dyes are the most frequently used synthetic dyes; however, they are not environmentally friendly because Ru is a heavy metal [6]. Such dyes are also very expensive because of the scarcity of Ru. In contrast, natural dyes are readily available, cheap, non-toxic, environmentally friendly, biodegradable, easily extracted, and can be used without any purification. Since DSSC mimic the photosynthesis of green plants, chlorophyll can also function as a photosensitizer for DSSC. In fact, a report on chlorophyll as a photosensitizer on zinc oxide (ZnO) semiconductors was first published by Tributsch in 1972 [7].

It was hypothesized that natural dyes with higher anthocyanin concentrations, such as those

extracted from blueberries and black raspberries, have higher fill factors and efficiency. The chlorophyll (A) structure in Punica granatum peel extract resulted in a solar cell with a 1.86% conversion efficiency [16].

A solar cell or photovoltaic cell is an electrical device through which the photovoltaic effect directly converts light(photons) energy into electricity while illuminated by sunlight (Bagher et al., 2015). Photovoltaic devices are based on charge separation at the interface of different conduction mechanisms of two materials, one of the regions having electron-hole majority carriers. A sufficient and clean energy supply is closely related to global stability, economic growth, and a good quality of life.

A typical DSSC consists of five components: a substrate (i.e., a glass plate coated with fluorine-doped tin oxide, FTO), a semiconductor monolayer such as TiO_2, ZnO, or SnO_2, and a dye sensitizer, which constitutes the photoanode, an electrolyte containing a redox couple, and a counter electrode.

Liquid electrolytes (LEs) prepared by dissolving a redox couple in low-boiling organic solvents are conventionally used in DSSC because of their easy preparation, high conductivity, low viscosity, and good interfacial wetting between the electrolytes and electrodes, thus achieving high conversion efficiency. Liquid electrolytes have limitations, including packing difficulties, leakage, and corrosion of electrodes.

Over time, polymer electrolytes (PEs) have been used to overcome the difficulties associated with liquid electrolytes. Starch is an easily available biopolymer. However, the problem with using a starch-based biopolymer electrolyte in DSSCs is the possibility of the formation of a starch–iodine complex because the commonly used redox couple in DSSC is iodide/triiodide. When starch comes into contact with I_2 in the presence of atmospheric moisture, iodine molecules are inserted into the cage-like structure of amylopectin and form an array of amylose chains, forming a starch-iodine complex (Figure 1), which leads to the unavailability of free iodine in the electrolyte and significantly affects the conductivity of the electrolyte. Hence,

A cross-linking approach was adopted to prevent the formation of the starch–iodine complex. Crosslinking of starch restricts the insertion of iodine molecules into the starch polymer chain, making iodine available for ionic transport. Three different procedures are adopted for cross-linking

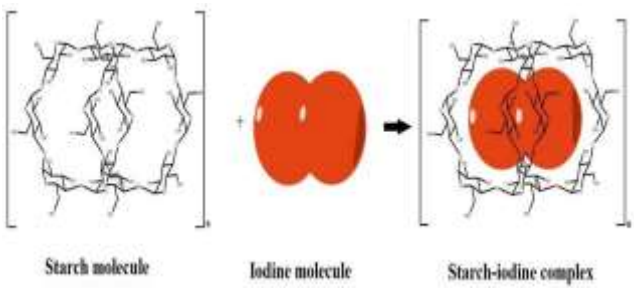

Quazi solid starch gel electrolyte (QSGE) bula allows the movement of ions without the need for a liquid or soft membrane separating the electrolyte. Owing to their hard matrix, solid electrolytes have low conductivity, and their conversion efficiencies are very low when compared with liquid electrolytes. Starch gel electrolytes (SGEs) possess both the cohesive properties of a solid and the diffusive properties of a liquid, and they have a low vapour pressure, which assures long-term stability and better efficiency Thus, this project was expected to add scientific information to academics about

indigenous plants potential for DSSC device technology

1.2. Statement of the Problem

The basic challenges related to the development of photovoltaic devices from both theoretical and experimental perspectives are as follows: narrowing the gap between the present experimental and theoretical efficiency limits (Harriet Kung, 2005); issues of low stability, low light absorption, liquid electrolyte leakage problems, and conversion efficiency (Ibn-Mohammed et al., 2017); low interaction between the semiconductor (here in TiO_2) and the dye photosensitizer (Ahliha et al., 2017); and the transport of photo-injected electrons competing by recombination (Wang & Chen, 2014). This study was conducted to demonstrate the development and evaluation of chlorophyll-synthesized solar cells as a mechanism to increase the conversion efficiency of solar cells and narrow the gap between theoretical and experimental research, in addition to providing scientific information about DSSCs.

1.3. Objectives of the Study

1.3.1. General Objective

The main objective of this study was to develop and evaluate chlorophyll synthesized solar cell by experimental study on natural dye extracted from Azadirachta indica for the TiO_2 based DSSC's

1.3.2. Specific Objectives

The Specific Objectives of this study were as follows:

- The optical properties of chlorophyll-synthesized solar cells and natural dyes extracted from Azadirachta indica were evaluated using XRD and FTIR methods.
- To examine the electronic properties (bandgap) of Azadirachta indica leaves.
- To investigate combined effect of starch gel and potassium iodide electrolyte effect on chlorophyll synthesized solar cells

1.4. Scope and Limitations of the Study

The aim of this study was to evaluate the potential of natural dye(Azadirachta indica) leaves as photosensitizers for the evaluation of chlorophyll-synthesized solar cells. The following chemical and materials were purchased from a market: Commercial standard TiO_2 paste, and starch gel. Natural dyes (Azadirachta indica) were used, and the optical properties of the dyes were characterized using XRD and FTIR spectroscopy. The DSSCs were fabricated, and J–V characterization was performed using Microsoft Excel. Thus, we checked the consistency of the derivate and computational results with the absorption spectra, FTIR, and device conversion efficiency.

CHAPTER TWO

2. Literature Review

2.1. Type of solar cells

Photovoltaic (PVs) solar cell technologies can be classified into different types based on various perspectives. For instance, based on overall device structure and architecture (wafer-based or thin-film based solar cells) based on generation (first, second and third generation solar cells) and based on the primary active material (silicon, semiconductor compounds and emerging/novel materials) (Ibn-Mohammed et al., 2017). Figure 1 shows a schematic representation of solar cell classification based on the primary active material.

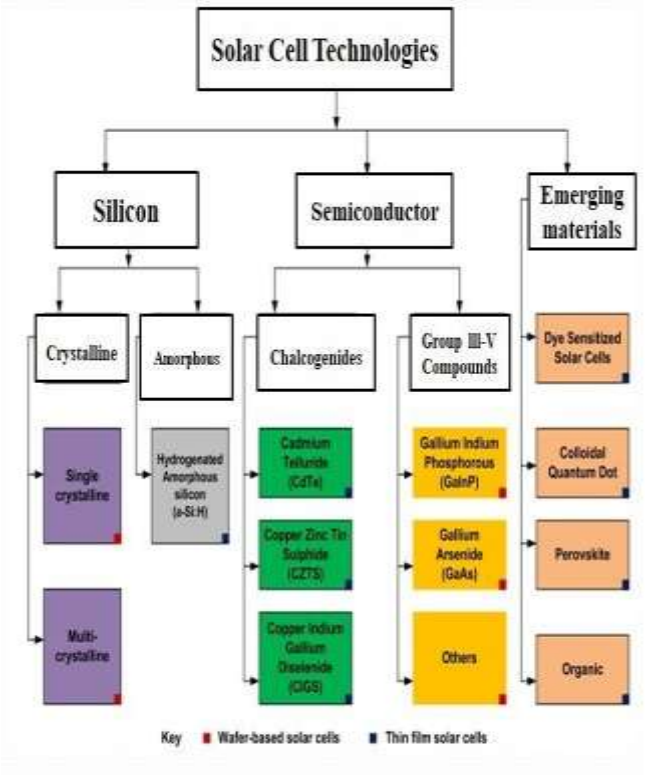

Figure 1: Classification of Solar Cells Technologies

Solar cell devices can be grouped into five major classes and 29 subclasses, as shown in Figure 2.

1) Multijunction cells,
2) Single-junction gallium arsenide cells,
3) Crystalline silicon cells,
4) thin-film technologies, and 5) emerging photovoltaics.

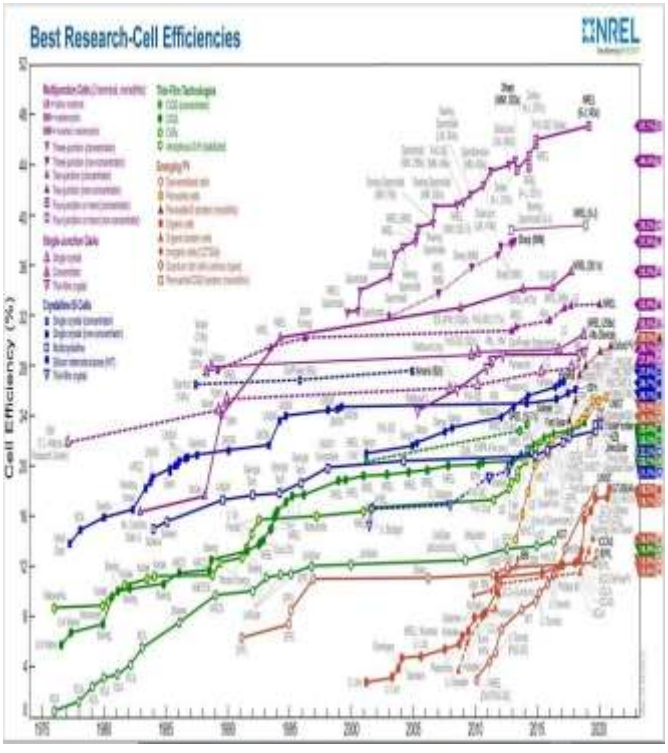

Figure 2:Best Research-Cell Efficiency Chart (NREL, 2022)

As shown in Figure 2, the DSSCs cell efficacy reached approximately 13% in 2091-2020. However, there is still a large gap between

multijunction solar cells (47.1) and four-junction solar cells.

2.2. Dye Sensitized Solar Cells (DSSCs)

Dye sensitized solar cells (DSSCs) are recently emerged as "third generation solar cells" that differ from commercial silicon-based solar cells, due to separation functions of both the light absorption and carrier charge transport system (Cari et al., 2016).

DSSC have four basic components: a photoanode, photosensitizer dye, redox electrolyte as a charge transport medium, and photocathode (Ahliha et al., 2017). DSSCs absorb and directly convert visible light into electricity upon the photo-electrochemical principles. It is based on the sensitization of wide band gap semiconductors used as electron carriers, which are sandwich-like structures formed by a photo-sensitized anode, a dye, an electrolyte, and a cathode (Zulkifili et al., 2015).

Table 1:: Comparison of Dye-Sensitized Solar Cell (DSSC) and Silicone Based Solar Cell

No.	**Characters**	**Silicone**	**DSSC**	**References**
1	Generation	First	Third	(Wahidah et al., 2018)
2	Raw Materials Cost	Expensive	Cheap	
	Raw Materials abundance	limited	Ample	(Chandiran et al., 2014)
3	Transparency	Opaque	Transparent	(Ebrahim, 2011)
4	Production Process	Complex	Simpler	
5	Power Generation Cost	High	Low	
6	Power Conversion Efficiency	High	Low	
7	Color	Limited	Numerous	
8	Lifetime	Long	Short	(Ahliha et al., 2017)
9	Eco-Friendly	Toxic	Non-Toxic	(Lee & Yang, 2011).
10	Weight	Harvey	Light	(Rossi et al., 2017)

2.3. The Role of Nanomaterials for Solar Cells

Nanotechnology is the manipulation of materials at the nanoscale from 1 to 100 nm. Nanotechnology applications have been verified in interdisciplinary fields such as physics, biology, chemistry, informatics, electronics, energy, and materials sciences (Shayan, 2020). Nanomaterials improve the optical and electrical properties of solar cells, including antireflection, light absorption, photocurrent, fill factor, and device efficiency (Amalathas, 2019). They also increase light absorption by reducing surface reflection and transmission and modify the optical properties of solar cells; however, better quality production systems and careful engineering are required (Amalathas, 2019). The foremost research goals in molecular nanotechnology are the design, modeling, and production of molecular machines and devices (Leach & Merkle, 1991). It has been reported that the conversion efficiency of DSSCs with an orderly interconnected nanosheet anode is approximately 27% higher than that with a nanoparticle anode (Wang & Chen, 2014). A nanomaterial helps increase the surface-area-to-volume ratio of the materials. This leads to an increase in the number of interfaces and the rate of electron adsorption and transport from the biomolecule to the electrode.

Nanomaterials can advance the fabrication and distribution of solar devices as well as the efficiency of solar energy generation and storage, similar to energy storage batteries, and boost electrolyte efficiency. Currently, the applications of nanotechnology in solar cells are in the research process stage, with remarkable promise in improving the efficiency of solar cells. Specifically, novel ideas have been discovered in the areas of self-cleaning, antireflective nano-coatings, thermo-photoelectric cells, hot carriers, solar cell generation, spectrum modulation, middle band and multi-generation, and nanocatalysts.

2. 4. Applications of Solar Cell Technologies

In general, solar cell technology products are entering the market with numerous applications, such as hand bags (Hug et al., 2014), daily goods and wearable clothes (Jasim, 2011), and building integrated PV panels (Wilson et al., 2020). Argo photovoltaics, solar PV thermal systems, solar-powered sesalination, solar trees, solar carports, and Floating PV systems panels, solar roof cars, hand watches, eye glasses (IRENA, 2019), landing obstruction lights for airports, water pumping for irrigation, power sources for homes and commercial buildings, perimeter alarm transmitters, electronic border fences, intrusion alarms for security, highway signs, portable backpack radios, remotely located, unmanned electronic surveillance systems, educational TV broadcasting, railroads, radio relay stations, navigation aid sensors, ocean-based earthquake warning systems, emergency alarm transmitters, communication satellites, and space-based missile surveillance and reconnaissance systems (AR). Jha, 2010).

2.5. Thermodynamics Properties of Sunlight

The surface of the sun is the source of the solar radiation emission that obeys the rules of a blackbody with a temperature of approximately 6000 K. In semiconductor materials, photons of appropriate energy can only be absorbed and generate electron-hole pairs. Thus, it is essential to consider the spectral distribution of the solar radiation. Terrestrial solar radiation is limited by factors such as light intensity and spectral distribution, which are driven by both the position of the sun and the Earth in the sky (Oliveti et al., 2014). Overall, the device generates electric power from light without permanent chemical transformation.

The optical air mass (AM) is the actual path length of sunlight divided by its minimum distance. An air Mass is a concept that describes the effect of a clear atmosphere on sunlight, which is equal to the direct beam path of relative length passing through the atmosphere. Air Mass Zero (AMO) is the radiation in the actual spectrum of sunlight measured outside the Earth's atmosphere (extraterrestrial spectrum). Mathematically, the irradiance at AM0 is 1361 $W \cdot m^{-2}$, which is known as the solar constant. The air Mass 1.5 G (AM1.5G and AM1.5D) solar spectrum is the standard terrestrial (on the earth's surface) reference solar spectrum on a clear day, which corresponds to an angle of 48.2°. with a total irradiance of 827 $W \cdot m^{-2}$, and is used for solar cell and module calibration in industry at a global irradiance (G) of approximately 1000 W/m^2 or 1 kW/m^2 (Frost, 2015) (Oliveti et al., 2014) (Conibeer, Gavin, and Willoughby, 2014) (Antonio Luque and Hegedus Steven, 2003).

The optical air mass is unity while the Sun is at its peak and the spectrum is called the air mass 1 (AM1) spectrum. When the Sun is at an angle θ with the peak, the air mass is calculated using Equation 1 (Oliveti et al., 2014).

$$AM: = \frac{1}{cos\ \theta} \quad \ldots\ldots\ldots\ldots\ldots\ldots\ldots\ldots\ldots\ldots\ldots\ldots\ldots\ldots\ldots\ldots\ldots\ldots\ldots\ldots (1)$$

Apart from clear-sky light, the sources of solar radiation losses are air molecules (H_2O, O_2, and CO_2), dust particles, and/or aerosols in the atmosphere. They are wavelength-selective because of scattering and absorption of sunlight (Oliveti et al., 2014). Figure 4 shows the radiation spectrum of sunlight.

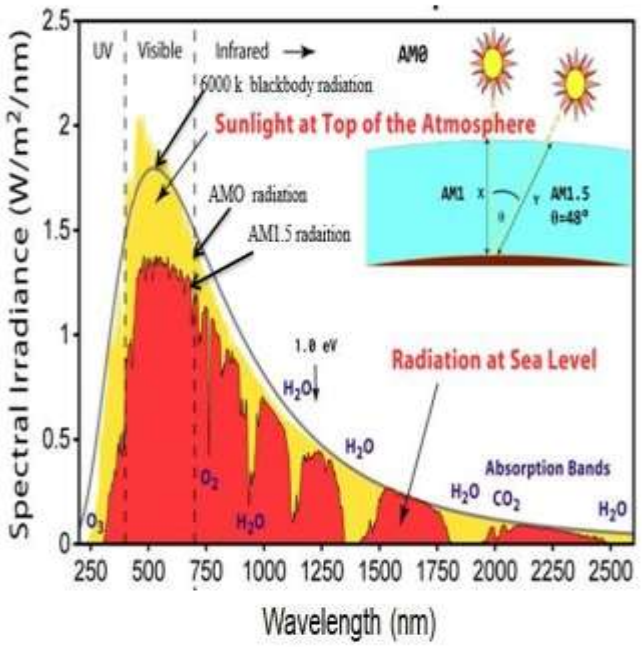

Figure 3:Solar Radiation Spectrum (Oliveti et al., 2014)(Frost, 2015).

2.6. Basic Principle and Operation of DSSCs

Light absorption is the first phenomenon in Photovoltaic cells, especially DSSCs, and its main goal is to maximize photon-to-charge conversion efficiency (Concina & Vomiero, 2014). As shown in Figure 4, dye-sensitized

solar cells are made up of four critical components: a working electrode (WE) or photo-electrode (PE) (herein; TiO_2 based photo-anode), a platinized or graphite counter electrode (CE), a photosensitive dye, and a redox-mediator electrolyte (herein, I^-/I^-_3 electrolyte solution) ((Jasim, 2011)(Antonio Luque & Hegedus Steven, 2003)(Gong et al., 2017)(Iqbal et al., 2019)(Sarker et al., 2015)). The fifth most important part is the substrate glass of the Transparent Conducting Oxide (TCO) layer covering the top and bottom of the cell (Mahalingam & Abdullah, 2016). Each part of the DSSC depends on numerous different materials. By changing device components such as the oxide's particle size, film thickness, electrolyte composition, electrodes, or photosensitizer dye, comparative changes are expected in the system (Iqbal et al., 2019).

The complete processes of chemical reactions that occur in a photovoltaic (PV) cell include absorption, separation, excitation, and accumulation of charges, respectively ((Iqbal et al., 2019) (Kumara et al., 2017) (Bagher et al., 2015)). The basic processes taking place in DSSCs can be explained from equation (7) through equation (10): 1) photoexcitation, 2) electron injection from the dye to the TiO_2, (3) electron transport to the anode, 4) dye regeneration by the I_3^- species, and 5) hole transport to the cathode, where a catalytic reaction occurs. In contrast, recombination processes may occur, which tend to inhibit fast exaction separation, charge transport, and collection, resulting in a decrease in photoconversion efficiency; 6) before charge separation and injection, non-radiative exciton recombination may occur; 7) charge recombination takes place between electrons at the oxide photoanode and I_3^- in the electrolyte; 8) furthermore, for dye regeneration, fast electron– hole recombination (Concina & Vomiero, 2014). Note that recombination and non-radiative relaxation of the photo-excited dye decrease the efficiency of the DSSCs. To overcome these challenges, electron injection and regeneration must be performed kinetically(Kumara et al., 2017).

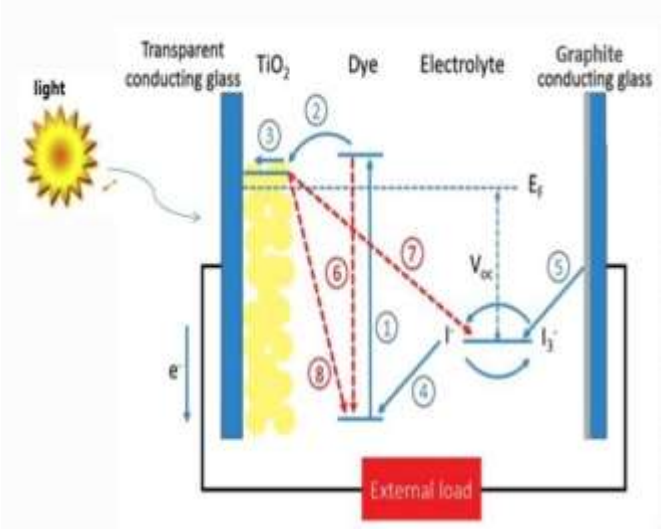

Figure 4:The complete processes of photo electrochemical reactions of a dye sensitized solar cell, In blue; light-to-electric power conversion, and in red, recombination (Concina & Vomiero, 2014).

An imaginary horizontal line at energy E_f, called the Fermi energy, represents the energy above which the probability of electron states being filled is under 50%, and below which the probability of electron states being filled is over 50% (Kitai, 2011). Electron excitation occurs at photon energies nearly equal to the bandgap ($E_{ph}=E_g$). There are two conditions that lead to half of the total energy conversion loss: when the photon energies are much lower than the band gap ($E_{ph}<E_g$) and when photon energies exceed the band gap ($E_{ph}>E_g$) (Oliveti et al., 2014).

1. (dye molecules) + hv − → (dye molecules) *…… ……..…..……Photo excitation (1)

2. (dye molecule) * → (dye molecule) + -e^- (TiO_2) ……Electron injection (2)

3. e^- (TiO_2) → e^- (wire) ……El ectron diffusion (3)

4. I_3^- +2e^- (counter electrode) → 3I^- ……..……Electron transfer to electrolyte (4)

5. 2(dye molecule) + +3I^- → 2(dye molecule) + I_3^- ……..……Dye regeneration (5)

6. (dye molecule) + +e^- → (dye molecule) ……. Recombination with dye (6)

7. I_3^- +2e^- → 3I^- ……..……Recombination with electrolyte (7)

8. (Dye molecule) * → (Dye molecule) ……..……Relaxation (8)

(Al et al., 2020)

Where**:** hv = photon (light); D = the ground state of the dye; D* = the excited state of the dye; D^+ = the oxidized state of the dye. e^-_{Cb} (TiO_2)=conduction band (CB) edge of the semiconductor (TiO_2), (Al et al., 2020) (Calogero et al., 2012).

2. 7. Basic Components of DSSCs

2.7.1. Photosensitizer Natural Dye

Light harvesting occurs in a photoactive dye molecule anchored to the surface of a semiconductor oxide (Noel et al., 2014). Photosensitizer dyes can be grouped into synthetic and natural dyes. They are required to have suitable visible light spectrum absorption, anchored chemical groups, and to inject electrons into the semiconductor surface. A number of natural dye pigments, namely flavonoids, beta-carotene, chlorophyll, anthocyanin, and tannin, are used as photosensitizer dyes in dye-based solar cells. The application of natural dye pigments has many advantages for DSSCs because they are easy to extract, biodegradable, nontoxic, abundant, and environmentally friendly (Zulkifili et al., 2015). The presence of hydroxyl and carbonyl groups facilitates the binding of dye to the TiO_2 surface (Prima et al., 2017). To achieve stable adsorption of dye onto the semiconductor substrate, Grätzel et al. reported that photosensitizer dyes are commonly designed to possess functional groups such as –COOH, $–PO_3H_2$, and $–B(OH)_2$ (Ghernaout et al., 2020). Furthermore, The chemical properties organic solvents that are more polar and contain R groups are more soluble than water used as a solvent for the preparation of photosensitize dye solutions (Ahliha et al., 2017). The excitation and injection of electrons from the ground state of the dye to the excited dye should be slightly similar to the band gap HOMO or LUMO of the semiconductors (Titanium Oxide with a band gap (3.2 eV) upon the carboxyl groups of

the dye to convert electrical energy (Wahidah et al. 2018). This indicates that extremely high or low excitation of electrons from the HOMO or LUMO of the photosensitizer dye molecules causes charge recombination and reduces conversion efficiency.

The working electrode or photoanode of DSSC is used as an electron transport medium to accept photogenerated electrons from the excited state of dye molecules and transfer them to an external circuit (Nurrida et al., 2017). The ideal photoanode is a single crystalline structure with a sufficiently large pore size, mesopores (high porosity with nanometer length scale), and high charge-carrier transport. The morphology of the electron-conducting photoanode is the main factor affecting the amount of surface available dye anchoring area required to allow ion diffusion in a solution-based electrolyte or pore infiltration on a solid-state hole conductor (Noel et al., 2014).

Photoanodes are made from nanostructured metal-oxide film semiconducting materials such as TiO_2, ZnO, SnO_2, Nb_2O_5, and NiO (Ghernaout et al., 2020); CeO_2, Bi_2S_3(Lai et al., 2015); In_2O_3, WO_3, ZrO_2, Ta_2O_5, and $SrTiO_3$ (Mahalingam & Abdullah, 2016) deposited on either a microscopic substrate or ITO coated with transparent conducting glass. Among these semiconductors, TiO_2 is the most promising material for solar applications owing to its high photoactivity, nontoxicity, low cost, easy availability, high quantum yield, and wide band gap (3.2 eV), which limits its photoactivity to ultraviolet irradiation (Cavallo et al., 2017).

Therefore, the TiO_2 layers were immersed in a photosensitive molecular dye solution. At the semiconductor surface, the nanocrystalline morphology provides a highly porous structure and large surface area of the electrode, increasing the covalently bonded dye molecules, light absorption, and energy conversion efficiency (Ghernaout et al., 2020). In DSSCs, n-type metal oxide photoanode than p-type metal oxide are better candidates for improving photocatalytic activity and efficiency such as TiO_2 nanocrystals. The electronic structures of these semiconductors have a filled valence band and empty conduction band (Cavallo et al., 2017). TiO_2 is an n-type semiconductor with three crystalline phases in nature: anatase, rutile, and brookite. The different structures of the TiO_2 phase lead to different properties (Lai et al., 2015). Nanocrystalline TiO_2 is a semiconductor with a large energy band (3-3.2 eV) or 380 nm in the transparent spectrum (Ahliha et al., 2017).

2.7.3. Electrolyte (Redox-mediator)

Solid-state, quasi-solid-state, and liquid electrolytes are the three major types of electrolytes applicable to DSSC. Its use assists in the regeneration of dye after electron injection, a (+) charge transport medium into the counter electrode (CE), and maintains the stability of the solar cell device (Kumara et al., 2017). It has been reported that the I^-/I^-_3 based liquid electrolyte is suitable for ion diffusion and infiltrates the TiO2 film well, exhibiting the highest efficiency among all DSSCs(Sanjay et al., 2018).

Many electrolytes have been reported, such as I^-/I^-_3, Br^-/Br^-, SCN^-/SCN_2, and Co (II)/Co (III), used as mediators in the form of gel, quasi-solid-state, ionic liquids, and liquids. Furthermore, electrolytes have five major constituents: redox couples, solvent-keeping elevated dielectric constants (for example, Acetonitrile, N-methyl pyrrolidine, and valero nitrile), additives that help to shift the conduction band of the semiconductor upwards and diminish recombination via back transfer to an electrolyte, which leads to an increase in the value of open circuit voltage (V_{OC}), decreased cell photocurrent (J_{SC}), and less injection driving force (e.g., 4 -Tertbutyl pyridine TBP). Consequently, the leakage factor of ionic liquids (ILs) is corrected using solid-state electrolytes and cations. A good electrolyte should have the following major features: the redox couple, long-term stability of chemical, thermal, and electrochemical and conductivity properties, non-corrosive device components, fast transfer of charge carriers, effective contact between both electrodes(PE and CE), and equivalent absorption spectra of an electrolyte with photosensitized dye molecules (Ghernaout et al., 2020).

2.7.4. Counter Electrode (CE)

Various types of CEs, such as metals and alloys, have transparency and flexibility. Fe Se, and $CoNi_{0.25}$, carbon materials e.g. carbon (C), conductive polymers, transition metal compounds, and hybrids e.g. carbonyl sulfide (CoS), Au/GNP . In addition to collecting holes from the hole transport materials, CE helps catalyze the reduction of the I^-/I^-_3 liquid electrolyte (Ghernaout et al., 2020). Optically transparent counter electrodes are used for light harvesting and practical applications such as windows, roof panels, and various decorative installations (Gong et al., 2017).

Graphene carbon is an exciting material with efficient electron transport, restricting the recombination of photo generated electron-hole pairs, but it lowers the bandgap energy of the device (Lai et al., 2015). Platinum () or carbon (C) doped films are frequently used in DSSC as a Counter Electrode (CE).

2. 8. J-V Characteristics of Solar Cell

The J-V characteristics of the solar cell device are shown in Figure 7. Electrochemical PV (EPV) cells operate upon the establishment of an electric potential difference between an n- or p-type semiconductor and redox electrolyte. This difference created an electrical diode structure. The current-voltage behavior of such junctions follows diode equations, in which the current flow in one direction across the junction is constant with voltage, whereas the current flow in the other direction across the junction increases exponentially with the applied voltage (Harriet Kung, 2005). The “peak watt” (Wp) rating is the output power (in watts) produced by a solar module illuminated when the sun is at a 42° elevation from the horizon (defined as air mass) under 100 mW/m^2 intensity, at high noon on a cloudless day, 25℃ ambient temperature, and a spectrum that relates to sunlight that has passed through the atmosphere of standard conditions [or AM] 1.5. (Kung 2005)(Grätzel 2000). The photovoltage (V_{oc}) is determined by the potential difference in the Fermi level of the electrons in the conduction band and the redox

potential of the electrolyte. Similarly, the photocurrent (J_{sc}) was determined based on the incident light-harvesting efficiency (LHE), charge injection, and collection efficiency. Device efficiency can be maximized by optimizing each of these three parameters (V_{oc}, J_{sc}, and FF)(Gong et al., 2017).

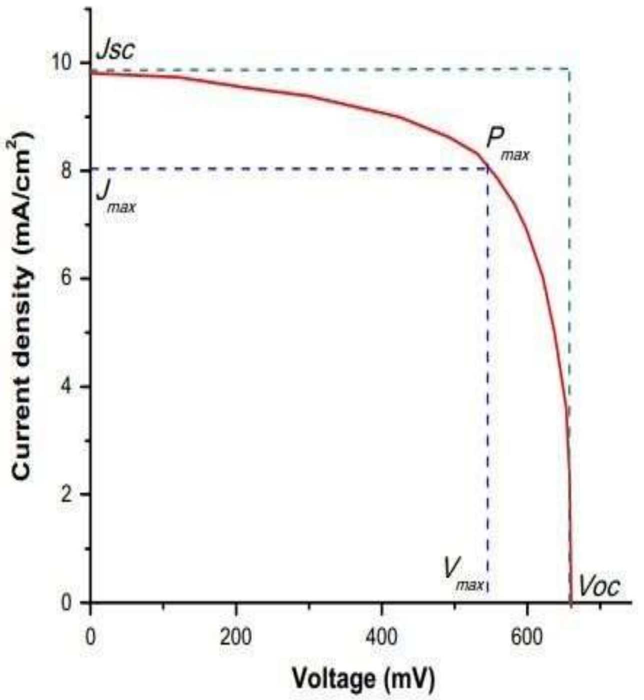

Figure 5: J-V characteristics of solar cell device (Kumara et al., 2022).

The increase in reverse current occurs due to optically generated electron-hole pairs that are swept across the depletion region to become majority carriers on either side of the diode. A diagram of the single-diode equivalent circuit is shown in Fig. 5.

Equivalent circuits and their variants provide information about a single cell and serve as powerful tools for analyzing DSSC modules. It avoids the bulky use of a number of physical and chemical parameters but instead projects the PV system as a combination of a minimal number of electrical circuit elements.

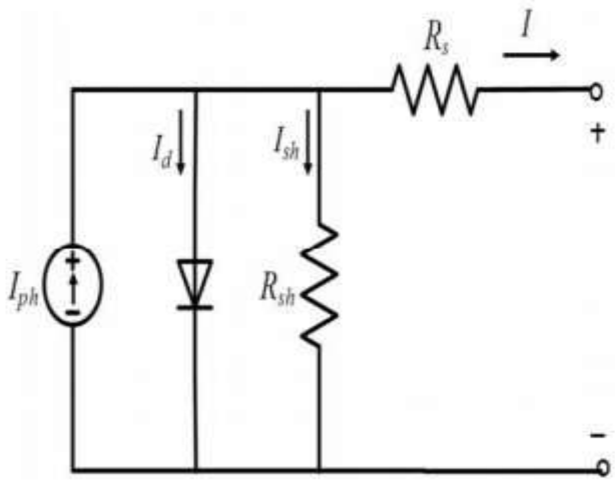

Figure 6: Diagram of single-diode equivalent circuit(Gong et al., 2017).

The diode model equation for solar cells relates the cell current density (j_{cell}) to the cell voltage (V_{cell}). A PV solar cell based on a single-diode model can be represented by an equivalent circuit under illumination (Cheknane & Hilal, 2008). When there is light, l_{ph}=0, the diode will be revised or dark diode, the reverse saturation current of the diode, and the parameters are extracted as follows (Harriet Kung, 2005): the dark current density (J_{dark} [amps/mm^2]), as a function of the voltage (V) applied to this diode (assuming ideal diode behavior), can be calculated by the equation below.

$$J_{dark}(V) = J_0\left(e^{\frac{qV}{kT}} - 1\right) \quad (7)$$

Where J_0 is a constant, q is the electronic charge (1.602 x 10^{-9}c), k is Boltzmann's constant, and T is the temperature (K).

If a diode is illuminated, additional charge carriers are created upon the absorption of light. These carriers create an additional current flow across the junction and must be added to the dark current to obtain the total current in the system. For illumination with light of many different wavelengths, the total photo-induced current can be

calculated by summing (i.e., integrating) the contributions to the current from excitation at each wavelength (Ebrahim, 2011).

For a given incident light intensity, at a given temperature, the relation between external current and voltage characteristic of the one-diode equivalent circuit with the series resistance and the shunt resistance described as a current source in parallel with the junction calculated as follows (Cheknane & Hilal, 2008) in Equation below

$$J_{cell} = J_{ph} - \frac{V_{cell} + J_{cell}R_s}{R_{sh}} - J_o\left[\exp\left\{\frac{q}{mk_BT}(V_{cell} + J_{cell}R_s)\right\} - 1\right] \ldots\ldots\ldots\ldots (8)$$

where J_{ph} is the photo-generated current density, j_0 the dark saturation current density, m the ideality factor, R_s the series resistance, R_{sh} the shunt resistance, k_B the Boltzmann's constant, q the elementary charge, and T the absolute temperature. Thus, the ideality factor m was recognized as the inverse of the transfer factor ßa(Sarker et al., 2015), which considers the deviation of the diodes from Shockley diffusion theory (W-function et al., 2014). For highly efficient solar cells, the shunt resistance must be very high to prevent current leakage, whereas the series resistance must be very low to obtain a sharp rise in the forward current. In this case the total current density can be determined using Equation 9

$$J_{cell} = J_{ph} - J_o\left[\exp\left\{\frac{q}{mk_BT}(V_{cell} + J_{cell}R_s)\right\} - 1\right] \ldots\ldots\ldots\ldots (9)$$

Note the sign convention of $V < 0$ and $I > 0$ in the potential range of 0 to the open-circuit voltage (Voc). Furthermore, an I-V curve based method helps derive the equivalent circuit parameters of DSSCs (Gong et al., 2017).

The Open-Circuit Voltage (V_{OC})

The Open-Circuit Voltage (V_{OC}) corresponds to the forward bias voltage at which the dark current density compensates for the photocurrent density. The value of V_{OC} depends on the saturation current density of the solar cell and the photogenerated current. The saturation current density J_0 depends on recombination in the solar cell. Therefore, V_{OC} is a measure of the amount of recombination in a device. Because no current flows in the open circuit, the Open-Circuit Voltage (V_{OC}) for the ideal device is obtained by setting J(V) = 0 (Ebrahim, 2011); for the temperature effect, under open-circuit conditions, the Open-Circuit Voltage (V_{OC}) can be calculated using Equation 10.

$$V_{oc} = \left[\frac{KT}{q}\right] \ln\left[\frac{I_{ph}}{I_0} + 1\right] \ldots\ldots\ldots\ldots\ldots\ldots\ldots\ldots\ldots\ldots\ldots\ldots$$

In this case, V_{OC} is directly proportional to the temperature.

CHAPTER THREE

3 Materials and Methods

3.1. General Summary of Research Flow Diagram

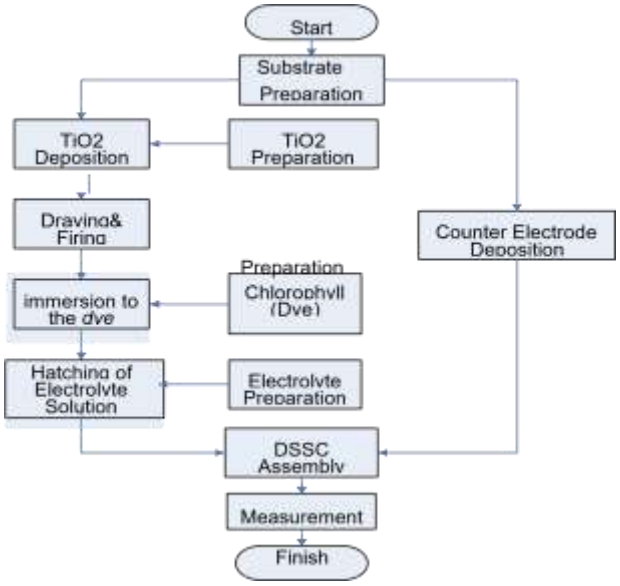

Figure 7:The general summary of research works conducted in the laboratory

3.2. Materials

3.2.1. The Starting Material of Natural Dyes

The Starting materials of Natural dye were Azadirachta indica Leaf

Figure 8:Azardinchita indica leaf.

It was smashed into fine small forms and mixed with ethanol in 10 g of Azardinchita indica leaf with 50 ml of ethanol and mixed well in a mortar and pistil until the color was formed.

Figure 9:Azardinchita indica leaf smashed in a mortar

3.2.2. The Starting Material of Transparent Glass Substrate

Macroscopic slide glass (25 mm × 75 mm) and insulator glass were obtained from the laboratory. It was coated with tin oxide to make it more conductive.

Figure 10:microscopic slide glass substrate (25mm x 75mm)

3.2.3. The Starting Material of TiO_2 Nanoparticle

The figure below shows the commercial standard transparent and reflective TiO_2 nanoparticle pastes.

Figure 11:Commercial Standard TiO2 pastes

3.2.4. The Starting Material of Liquid Electrolyte

In this work, a commercial standard couple of potassium iodide liquid electrolyte solutions was obtained from the School of Chemical Engineering Laboratory. Then, the electrolyte solution was placed between the Counter Electrode and dye-soaked photoanode.

3.2.5. The Starting Material of Photoanodes

The Standard Starting material was microscopic slide glass plates (75 mm x 25mm) coated with tin chloride to make it conductive

A) B)

Figure 12::

A) Peace of microscopic glass substrate Glass Substrates (75 x 25mm) and B) microscopic substrate glass coated with tin chloride to make it conductive glass

3.2.6. The Starting Material of Counter Electrode

A piece of microscopic glass slide plate (75 mm × 25 mm) was used as the counter electrode substrate. Carbon from the burning of candle smoke was used as the counter electrode.

3.2. 7. Chemicals

Solvents and reagents were obtained from the School of Chemical and Material Engineering Laboratory. Ethanol (96%) and distilled water were obtained from the School of Chemical Engineering Laboratories.

3.2. 8. Laboratory Instruments

Numerous critical instruments and tools applied in laboratories are listed below: oven-dry (300 ℃), furnace (430 ℃), Hot-plate, Analytical balance, digital multimeter, thermometers, glass rod, thermoplaster, and steel binder clips. Three characterization instruments were used: a UV–vis spectrophotometer (Hack6000), Fourier Transform Infrared (PerkinElmer®, Germany) spectrophotometer, and X-ray diffraction (XRD). These were applied to measure the absorption spectra, crystal size, and functional groups of the photosensitized dyes and to estimate the photoelectric conversion efficiency of the solar cells under standard AM 1.5 G solar radiation at 26 °C.

3.2.9. Characterization Parameters

This study includes the optical properties of natural dyes, such as absorption spectra and FTIR. Electrical properties of the DSSC devices included four device efficiency parameters Such as J_{sc}, V_{oc}, FF% and η%.

3.3 Methods

3.3.1. DSSC Device Fabrication Process

TiO_2 based DSSCs can be prepared from microscopic glass slides coated with tin chloride, TiO_2 nanoparticle pastes, graphite carbon, potassium iodide liquid electrolyte, and starch gel electrolyte to maintain stability. and chlorophyll-synthesized natural dye was extracted from Azadirachta indica leaves.

These components were assembled in the following steps, as shown in Figure 13.

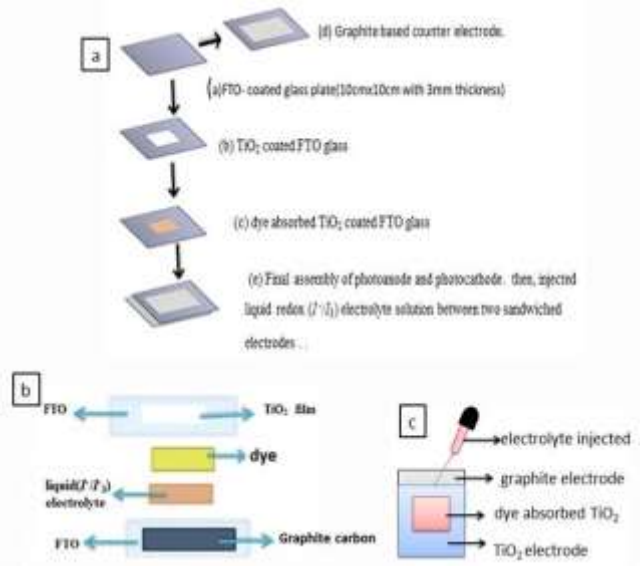

Figure 13:DSSC Fabrication Process: A) Overall Production Steps; (B) The Four Basic Components of Single Cell Device and (C) Assembled Single Cell Device

.

3.3.2. Preparation of Chlorophyll synthesized Dye Solution

Chlorophyll-synthesized natural dye was extracted from Azadirachta indica leaves using ethanol as a solvent. During the process, the dye solution container glasses were covered with aluminum foil and placed in a dark room to prevent damage from light exposure, which caused the dye efficiency to decrease (Godibo et al., 2014).

3.3.3 Research Design

Figure 14 illustrates the research design of this study. Precursor solution was used to fabricate

(create) titanium precursor solution titanium thin film, which was used as a block layer for the titanium paste and the candle smoke counter electrode (CE). The thin film with the titanium paste was immersed in chlorophyll dye extracted from a local plant leaf (neem leaves) using ethanol

as the solvent extraction and assembled in the DSSC.

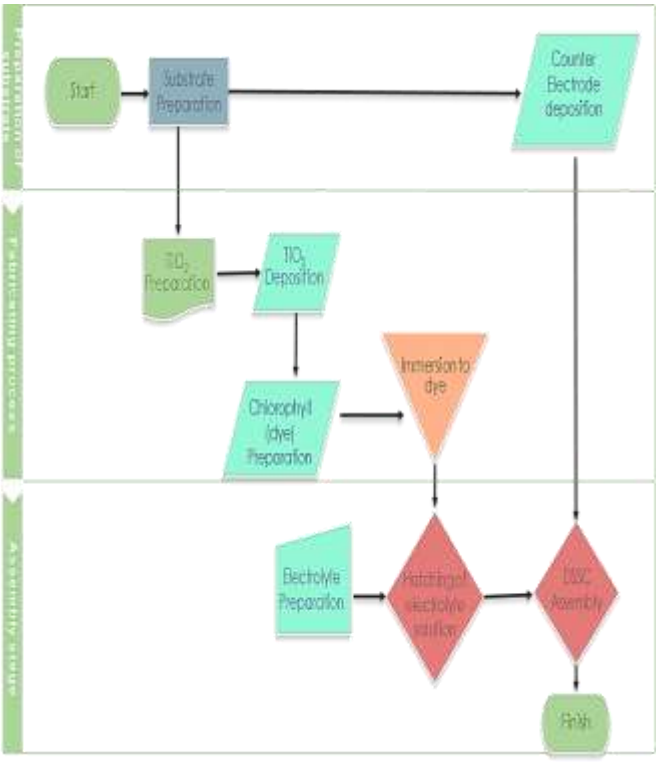

Figure 14: Schematic of the assembled DSSC research design.

3.3.4 Cleaning of Microscopic slide substrate and determination of the conductive side of microscopic slide substrate after cleaning

The microscopic slide glass substrates were soaked in ethanol for 2 min and washed with ethanol. The glass substrates were then rinsed with deionized water. Thereafter, it was air-dried for 10 min.

After cleaning the microscopic glass slide substrate, one side of the glass was coated with tin chloride to make it conductive, and the conductive side of the glass substrate was determined using a multimeter. The meter was set to measure Ohms, both leads were placed on one side of the slide, and the measured resistance was near zero, which was the conductive side.

The precursor solution was coated by hand using a stirrer, and the spreading of titanium paste and Candle smoke paste onto the microscopic slide substrate was performed on the conductive side of the microscopic slide substrate. This is the reason for determining the conductive side of the microscopic slide substrate after cleaning.

3.3.5 Preparation of Titanium precursor solution and coating of microscopic slide substrates.

The Molecular Precursor Method (MPM) was used to prepare the titanium solution. 10.00 g titanium was added to 100.00 g of ethanol.

After the successful preparation of the titanium solution, it was used to prepare the titanium thin film. The Microscopic slide substrate was cleaned, and the conductive side was determined as outlined in Section 3.2.1. Thereafter, the precursor solution was coated onto the conductive side of the microscopic slide substrate, as indicated in Scheme 2. Hand coating using a stirrer is a method of fabricating thin films that are used to deposit ultrathin films on substrates. This was done by allowing a sufficient precursor solution to spread evenly on the glass substrate. Next, the thin film was heated at 300 ℃ for 15 min in a heating pan. Heat treatment was performed to eliminate organic ligands from the resultant precursor thin films. The resulting thin film was preserved for use as a blocking layer.

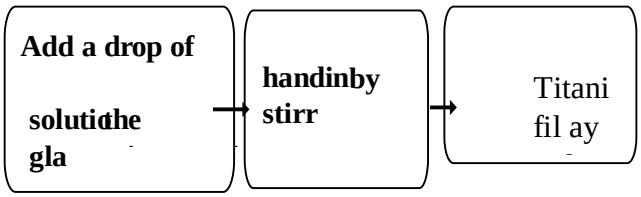

Scheme 2 hand coating by stirrer titanium solution on microscopic slide substrate.

3.2.6 Preparation of Candle smoke paste

Candle smoke paste was used to prepare carbon paste. Candle smoke was used to coat the cathodes. The conductive part was used, and candle smoke was used until a dark carbon paste was obtained.

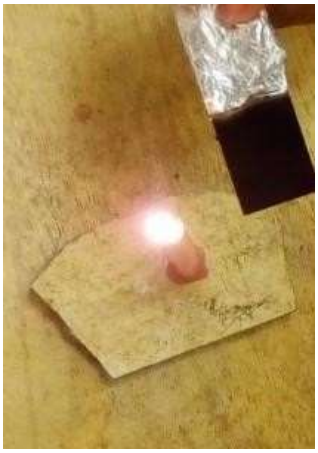

A)

B)

Figure 15:A) candle smoke making process in the lab for the cathode part B) candle smoke

3.2.7 Fabricating TiO_2-Candle smoke structure

The microscopic slide substrate was cleaned, and the conductive side was determined as outlined in Section 3.2.1. On the fabricated titanium thin film (used as a blocking layer), paste was coated

Using a stirrer, a paste of the microscopic slide substrate was heat-treated at 300°C for 15 min.

3.2.8 Preparation of Titanium paste

5 g of titanium die oxide was mixed with ethanol (50 ml of ethanol in order to make Tio2 paste suspension and placed in the dark to prevent light penetration.

3.2.9 Preparation of Chlorophyll dye

Chlorophyll was extracted from the leaves of Azardinchita indica (neem leaves) to prepare chlorophyll dye. Neem leaves were obtained from Jimma on the JIT campus (Oromia Region). These leaves were crushed to a fine powder, 5 g of powdered dry leaves was placed in a beaker, and 30 ml ethanol was then added. The mixture was mixed using a mortar and stirrer, stored for analysis, and used to fabricate the TiO_2-Chlorophyll film.

Figure 16:azardinchita indica (neem leaf)

3.2.10 Fabricating TiO_2-Chlorophyll sandwich structure

The microscopic slide substrate was cleaned, and the conductive side was determined as outlined in Section 3.2.1. Titanium paste was coated on the surface of the titanium microscopic slide substrate (fixed with scotch tape), adopting doctor blade method (section 3.2.3), titanium paste was coated on the conductive side of the glass substrate (fixed with scotch tape). The glass with the paste was then dried in air at room temperature for over 4 h and then heated at approximately 420 °C for another 20 min to remove any inorganic residue. After 20 min, the mixture was allowed to cool to room temperature. Next, the chlorophyll dye was added dropwise (slowly) onto the surface of the paste using a pipette until it was completely covered with the dye. The sides of the glass with no paste were rinsed with ethanol to remove any residual dye from the glass substrate.

3.2.11 Preparation of the Iodide electrolyte

The triiodide electrolyte was prepared using Raihana's [50] method. Potassium Iodide crystals (30 g) were dissolved in 120 ml of distilled water. Potassium iodide (30 g) was added and the solution was stirred until it dissolved. This solution was stored as a KI/I_2 electrolyte solution in the dark for later use. The KI/I_2 electrolyte solution is sensitive to light and thus must be stored in a container where it does not react with light.

3.2.12 **preparation of the starch gel electrolyte**

Potassium Iodide crystals (30 g) were dissolved in 120 ml of distilled water. Potassium iodide (30 g) was added, and the solution was stirred until it dissolved and heated to 100c °C using a heating pan. Then, 30 g of starch gel (bula) was added to the solution until a starch gel was formed. This solution was stored as a starch gel electrolyte solution in the dark for later use. The starch gel electrolyte solution is sensitive to light and thus must be stored in a container where it does not react with light.

Figure 17:starch gel making process

3.2.13 Assembling TiO_2-candle smoke Chlorophyll sandwich based DSSC

The two fabricated (constructed) films, the TiO_2-Candle smoke structure and the TiO_2Chlorophyll structure, were assembled together in a sandwich form. A candle smoke structure was placed on top of the TiO_2-Chlorophyll structure. Plastic was used to seal the assembled sandwich-based DSSC with a clear adhesive. A small hole was left in the plastic seal for the injection of the electrolyte solution. After the complete assembly of the cell, defects were inspected. After inspection, a few drops of KI/I_2 electrolyte solution were injected into the cell.

Finally, the photovoltage of the assembled TiO_2 carbon smoke and TiO_2-Chlorophyll sandwich based DSSC was measured. Because

measurements were taken outdoors, solar radiation received by Jimma was used, which is kWh/m^2.

3.3.14 Dye solution magnetic stirrer machine

The dye mixing process was conducted using a magnetic stirrer for 30 min to achieve perfect mixing.

The laboratory magnetic stirrer is shown in Fig. 18.

Figure 18: Dye-mixing magnetic stirrer

As shown in Figure 18, this is indicated by the extended conjugation of the dye molecules. Greater elongation of the dye molecules leads to greater attachment to TiO_2, more photon absorption, and electron excitation, which are related to the increased conversion efficiency of solar cells.

CHAPTER FOUR

4.RESULTS AND DISCUSSION

4.1 RESULT

4.1.1 The fabricated titanium thin film

A transparent titanium thin film was obtained after annealing at 430 °C and removing any organic ligands for 30 min. This thin film was later used as the photoanode (blocking layer) and the counter electrode (blocking layer). Figure 19 shows the fabricated Ti films.

Figure 19:Titanium precursor solution

4.1.2The absorption spectrum of the fabricated TiO_2 on Microscopic substrate slide glass

TiO_2 prepared by MPM on microscopic conductive glass substrate absorb visible light, so that photo absorptions from solar energy may become more effective and can achieve higher efficiency. (glass), which shows an adsorption peak at 400 nm wavelength, adapted from Daniel

4.1.3Titanium dioxide paste fabricated thin film

The fabricated titanium thin film was later used to prepare a titanium dioxide thin film (figure 19). Titanium paste was deposited onto the fabricated titanium thin films using a stirrer. The substrate was then dried in air for 4 h. When the layer is too thin, cracks form; thus, the paste should be slightly thicker. However, cracks sometimes show complete drying of a substance. This can be seen in Figure 19, as the paste was completely dried after

4 h. Heat treatment was performed, and the paste was successfully deposited onto the precursor thin film after 4 h of air-drying. A white paste was obtained after heat treatment. The thickness of this paste layer can be referenced to the scotch tape fixed on the glass substrate when the coating was applied. This titanium dioxide paste film was used as the photoanode in the DSSC assembly.

Figure 20:Fabricated Titanium dioxide paste microscopic slide substrate after air drying.

4.1.4 Fabricated Candle smoke paste thin film

The thickness of the fabricated candle smoke paste layer can also be referenced to the thickness of the scotch tape that was fixed on the microscopic slide substrate when the candle smoke paste coating was applied. After successful mass deposition, the paste was bonded to the surface of the microscopic slide substrate by heat treatment, and a Candle smoke paste microscopic slide substrate (figure 20) was used as the CE in the DSSC assembly.

A) B)

Figure 21:A) Fabricated Candle smoke paste microscopic slide substrate (performed at 120 °C heat treatment). B) Candle smoke paste covered with aluminum foil after heat treatment.

4.1.5 Chlorophyll dye extracted from *azardinchita indica* leaves

Chlorophyll dye was successfully extracted from *Azardinchita indica* (neem) leaves. Ethanol was used as the solvent for the extraction of chlorophyll. Other solvents showed poor extraction of chlorophyll from the neem leaves. Chlorophyll is a pigment that absorbs green wavelengths, and hence, its green color. Chlorophyll extracted using ethanol displayed a dark green color. Figure 22 b shows the chlorophyll dye extracted using ethanol solvent.

A) B)

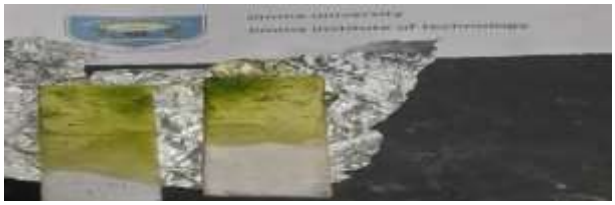

C)

Figure 22:a) Neem plant leaves b) Chlorophyll dye extracted in ethanol solvent from neem plant leaves. C) dye paste on microscopic slide

4.1.6 Infrared spectrum of the tin oxide on microscopic substrate glass

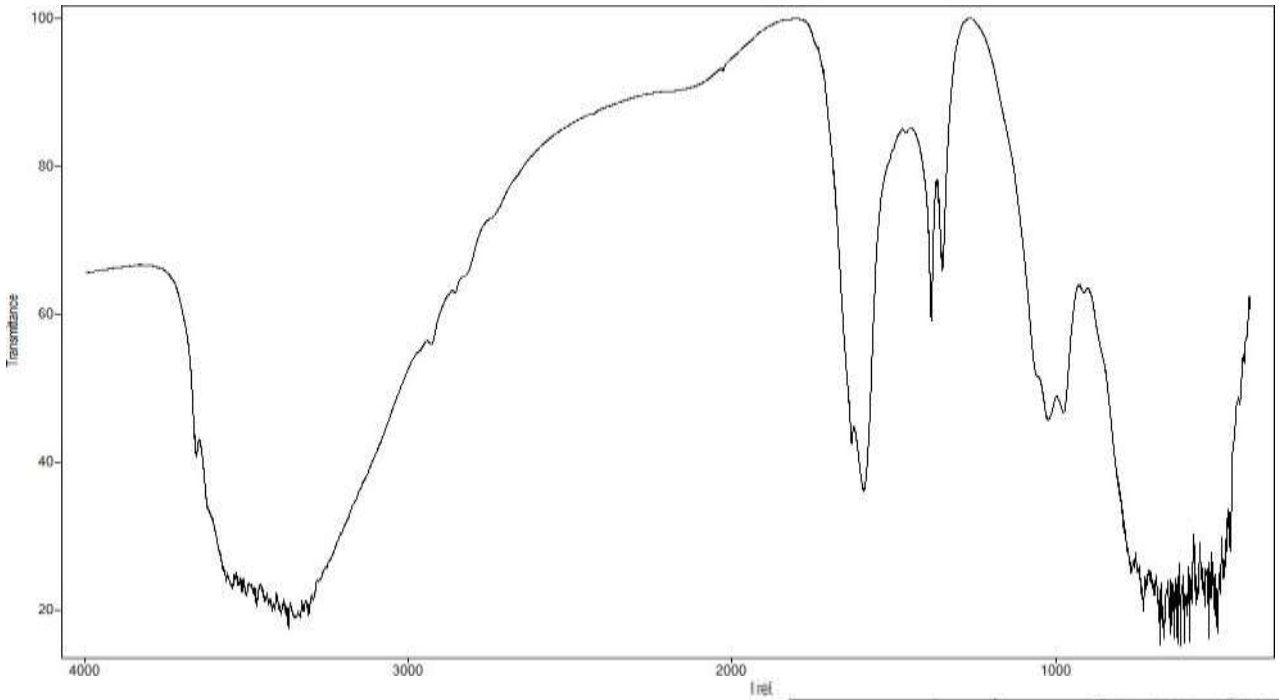

Figure 23:Infrared spectrum of the tin oxide on microscopic substrate glass

The above FTIR graph shows that tin chloride was converted to tin oxide and the band 659 cm^{-1}

which stands for Sn-O-Sn vibration we do have also OH absorbed on the Oxide surface as they are indicated at 1594.05 cm^{-1}, while 3554 cm^{-1}, indicates free OH groups that may be trapped from the atmosphere. These observations correlate with the structure of chlorophyll and are comparable with the data from the available literature; thus, it can be inferred that the extracted dye is indeed chlorophyll.

XRD of tin Oxide pattern Sno2 Diffraction pattern

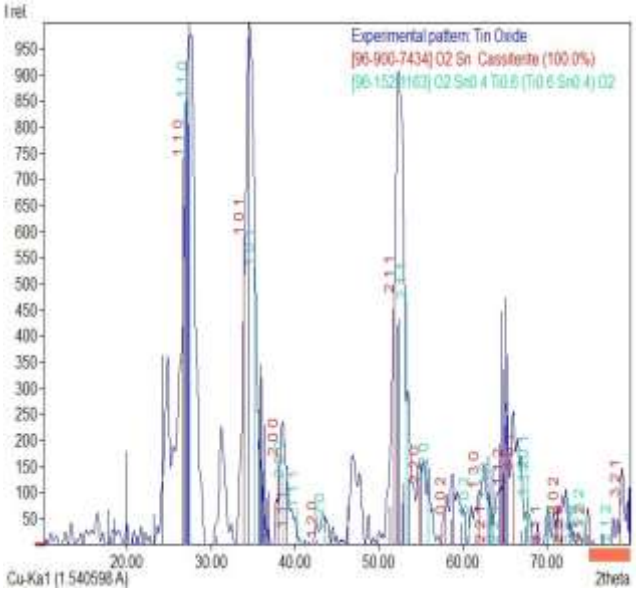

Figure 24:XRD Diffraction graph for tin oxide to determinate crystal size

4.1.7 Preparation of the Photoanode

The fabricated titanium dioxide paste layer was soaked in the chlorophyll dye extract for 20 min. Saking the soaking process for longer periods of time can give dye molecules ample time to adequately attach or bind to the surface of the nano porous titanium dioxide layer. This nanoporous

layer was simply used as a binding side for the extracted chlorophyll dye molecules.

Instead of dropping the thin films, the dye was added dropwise onto nanoporous titanium dioxide. This method allows sufficient adsorption of dye molecules onto the nano porous titanium dioxide surface compared to the conventional face-down dip.

Figure 25 shows the dioxide thin films soaked in chlorophyll dye. The striking green color can be clearly seen in figure 25; thus, we can conclude that the dye extract is indeed chlorophyll.

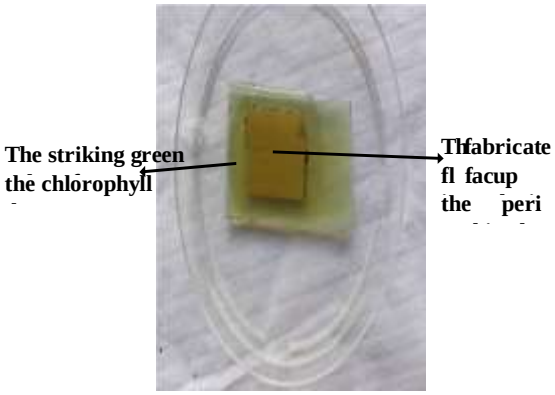

Figure 25:. Titanium dioxide thin film soaked in chlorophyll dye extract (face-up).

After the soaking period, the white nano porous titanium dioxide thin film displayed a green color (figure 25). This change in color was due to the adsorption of chlorophyll dye molecules on its surface. The resulting thin film was used as the photoanode for the cell.

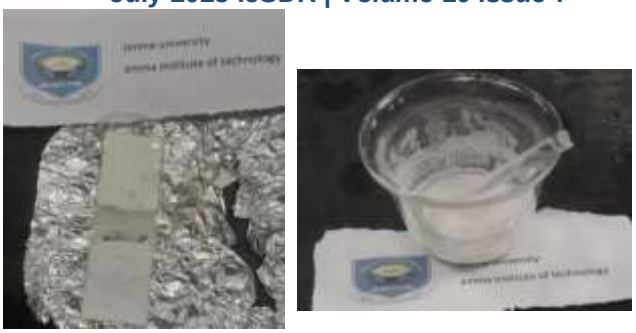

Figure 26:A) Chlorophyll dye sensitized titanium dioxide thin film. B) Titanium dioxide paste solution

4.1.8 Assembly of the DSSC

After all components of the DSSC were ready, the cells were assembled together. The active sides of the fabricated photoanode and the fabricated counter electrode faced each other. The fabricated titanium dioxide thin film and candle smoke-fabricated thin films faced each other. The space was left to accommodate the electrolyte. The DSSC design was (2.5 × 3) cm^2 (figure 27).

The electrodes can be squeezed together, and the electrolyte is introduced into the cell via the capillary effect. On the other hand, the electrodes can be wrapped, and the electrolyte is injected into the cell via holes made through the cathode.

The squeezing method is formally known as an open cell method because the internal area of the solar cell is uncovered or rather in air. Nevertheless, the electrolyte would not remain in the cell, and the cell would later dry. This method only applies to practical applications, and as a result, it faces a stability problem.

The second method, in contrast to the first approach, is the best choice because it is highly stable. The electrodes were joined together with a spacer to confine the electrolyte to the void. Although this is time-consuming, it enables the DSSC to operate for a longer period of time.

Since this study is research-based and would like to have results that could benefit the research community, the second approach seemed to fit this study. The second method (spacing) was used to assemble the DSSC.

In the space between the two electrodes, the electrolyte was injected into the DSSC via a hole left in the sealant. Once assembled, the cells were tested.

A multimeter was connected to the negative terminal of the photoanode (titanium electrode), and a positive terminal was connected to the counter electrode. The open-circuit voltage and short-circuit current of the solar cell were measured under full-sun illumination.

Smaller notches of microamperes and millivolts were also observed. In addition, the resistance of the cells was low. The current and voltage values of the cell were 250mA and 540 kV respectively. In contrast, the resistance of the assembled DSSC was 0.931MΩ. When the cell was covered with an A4 hard cover notebook (an opaque object), no sunlight or sunrays reached the cell, and the values dropped significantly. This indicates that the cell possibly performed best under direct sunlight.

After a week of assembly, photovoltaic measurements were performed again to determine the stability of the dye as well as the electrolyte. Similar results were obtained for the cells.

The assembled cells were tested using a solar motor. However, this cell did not power the motor possibly due to its size and exposed surface area which is 7.83 cm^2, considered very small.

Figure 27: Top view of the assembled dye-sensitized solar cell using candle smoke and Tio2 paste with a potassium iodide electrolyte Sandwich Structure.

4.1.9 The photovoltaic performance (photo-electrical conversion efficiency) of the assembled cell

The photovoltaic performance of the assembled DSSC was measured using a multimeter under direct sunlight. An external current flows when sunlight is incident on the anode side of the cell. For complete darkness, the cells were placed in a sealed container. This was done to test whether the cells could operate under no light.

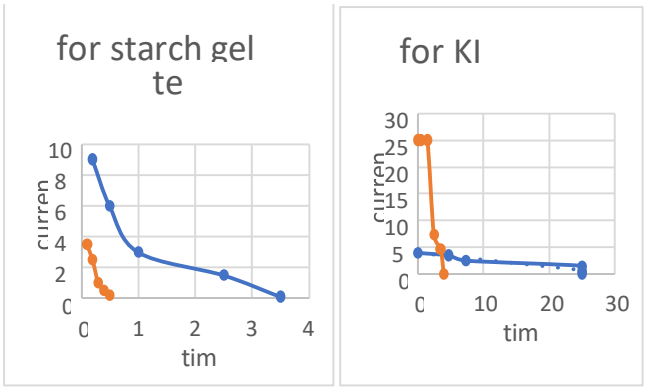

A) B)

Figure 28:A current vs time for starch gel electrolyte B) Current vs time relationship for liquid electrolyte (KI)

4.1. 10. Determination of energy band gap of the Dye Photosensitizer by relating temperature with resistivity test

Theoretically, the optical energy gap and absorption coefficient of the photosensitizing dye can be calculated using Equations 2 and 3(Kabir & Nazmus, 2019).

ln(R)=lna0+Eg/K*(1/T)

……empirical equation to calculate energy band gap

where R is the resistivity M ohum,T=Temperature,a0 is a constant parameter, and K=8.316×10^{-5} eV (Boltzmann constant, expressed in eV/k).

The amount of light absorbed by the dye molecules and the diffusion of the ejected electrons into the mesoporous TiO_2 film determine the overall performance of the DSSCs (Ghann et al., 2017).

4.1. 11 Infrared (IR) Absorption Spectra of the Photosensitized Dyes

FTIR is used to detect the material (gas, liquid, and solid) functional groups by which the infrared (IR) radiation (frequency) is absorbed and their intensity, and the result is expressed as % transmittance versus wavenumber (mm^{-1}) (Sharma et al., 2018). In the midinfrared region(4000-400mm^{-1}), there are two main types of vibrations: stretching vibrations

(m) and bending vibrations. Stretching vibrations (m) are vibrations along chemical bonds, which involve changes in bond length, and bending vibrations involve changes in bond angles, notably (din plane, pout of plane) (Berthomieu & Hienerwadel, 2009). The organic molecule binding vibrations in the solution were identified using a Fourier-transform infrared (FTIR) spectrophotometer (Prima et al., 2017).

The absorbance spectrum of a sample was calculated using Equation 4.

$$A = \log\frac{I_0}{I} \quad \ldots\ldots(4)$$

Where A absorbance, I_0 is the intensity in the background spectrum, and I is the intensity in the spectrum of the sample.

The absorbance could also be correlated with the concentration of molecules in a sample through the equation called as Beer's law, which is expressed by equation 5.

$$A = \varepsilon lc \quad \ldots\ldots(5)$$

where A is absorbance, ε is molar absorptivity, l is the path length, and C is the concentration of the sample.

The height or area of a peak in the absorbance spectrum is proportional to its concentration.

The y-axis of an infrared spectrum can also be plotted in units of percent transmittance (% T), which measures the percentage of light transmitted by the compound and can be calculated using Equation 6.

$$\%T = 100 \times \frac{I}{I_0} \quad \ldots\ldots(6)$$

Where % T, percent transmittance; I_0, intensity in the background spectrum; and I, intensity in the sample spectrum

4.1. 13. Computational Band-Gap Calculation natural dye molecules

The band-gap energies (HOMO–LUMO) of the natural dye molecules were calculated using an Excel spreadsheet to check the stability of all optimized structures and to obtain the trap point corrections to the total electronic energies (Ghann et al., 2017) (Dumbravă et al., 2012).

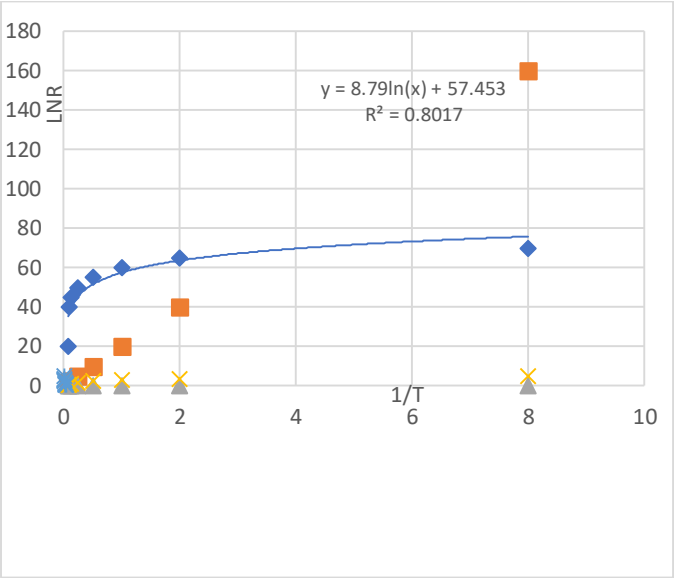

Figure 29:Tatianium di oxide conduction vs inverse temperature

Tio2 conduction vs temperature

Energy band gap for Tio2 semiconductor relation with thermal effect is calculated as ln R= lna0 +Eg/(kT) ,T=298K and K=8.61733326*10^-5ev/k, taken corrective factor 10%

Energy band gap =slope from graph 57.453

E=57.453*8.61733326*10^-5*298k = 1.475373*1.1=1.622871 ev

The gap energy of 3.2 eV which has been proven to be able to produce good efficiency. The smaller the particle size, the greater the surface area of the particle that binds with the dye sensitizer. The TiO_2 powder was produced using the coprecipitation method. TiO_2 was sensitized with dyes so that the range of the area of light absorption was wider because, without the dye, the range of the area of light absorption was only 360-380 nm. TiO_2 powder was converted into a solution form and then deposited on a conductive glass Indium Tin Oxide) measuring 3.0 x 2.5 mm which has good conductive properties for DSSC cells. This deposition was carried out by the hand stirrer coating method, in which a few drops of TiO2 solution were dripped on the conductive side of the glass and then rotated on the stirrer coating device until all sides of the glass were covered with solution. Glass deposited with TiO_2 solution was then dried for later immersion in a dye solution

Chlorophyll dye conductivity test by temperature dependance

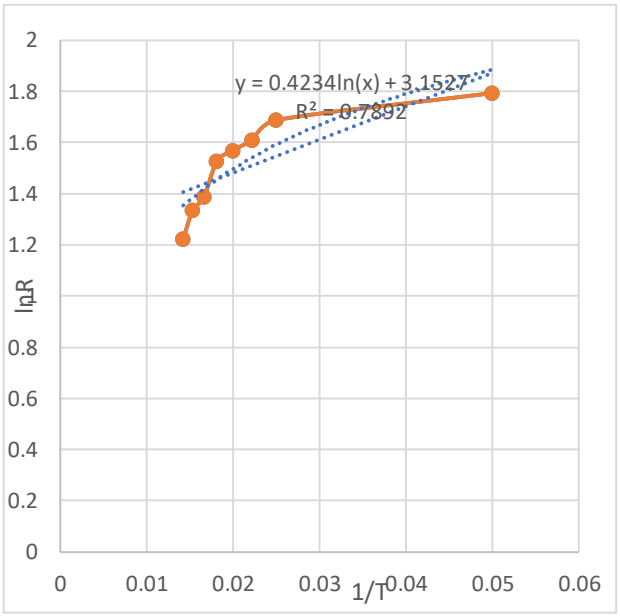

Figure 30:chlorophyll conductivity related inverse temperature dependance

The dye resistivity gradually and steadily decreased in the insulating glass material. Energy band gap for chlorophyll dye is calculated as

ln R= lna0 +Eg/(kT) ,T=298K and K=8.61733326*10^-5ev/k taken 10% energy band =1.023*1.1=1.1253 ev

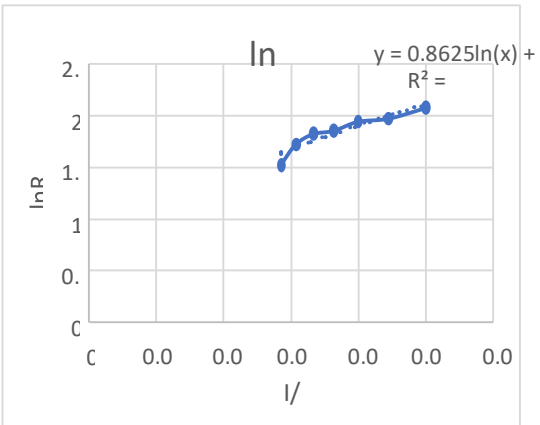

Figure 31:tin oxide conduction vs inverse temperature

Energy band gap for Sno2 relation with thermal effect is calculated as

ln R= lna0 +Eg/(kT) ,T=298K and K=8.61733326*10^-5ev/k

Energy band gap =1.768 ev taken as 10% of calculated Energy band gap(Eg)=1.1*1.768=1.9448ev

Voltage vs time for KI Test voltage vs time graph for starch gel

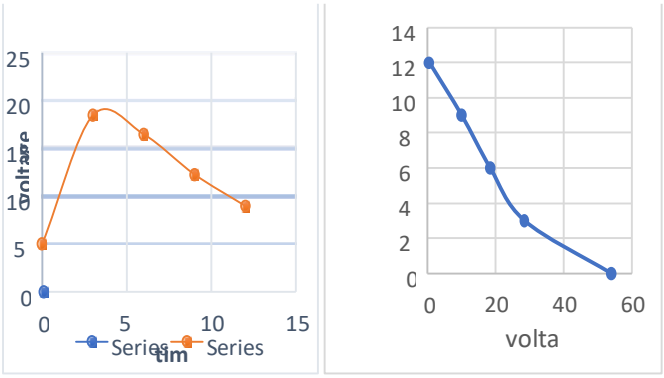

Figure 32:A) Voltage vs time for KI B) voltage vs time graph for starch gel

4.2 DISCUSSION

The results of sandwich cells with liquid electrolytes are shown in Fig.33, and loading was the same as when measuring cells with gel electrolyte. In measurement 1, when new cells were dropped with a liquid electrolyte at a loading resistance of 75 M Ω, the maximum current reached 250 μA in the first minute and then tended to decrease in the following minutes. However, the current remained large until the 15th minute and then dropped dramatically and was stable with very small current values. Then, it runs out in the 32nd min. Measurement 2 was performed on the same day, but electrolyte drops were needed again because without electrolyte drops, the current value did not reappear. It was conducted on the same day as measurement 1 because the next day, the sandwich cells would be oxidized or corroded, so that the quality was not good for measurement.

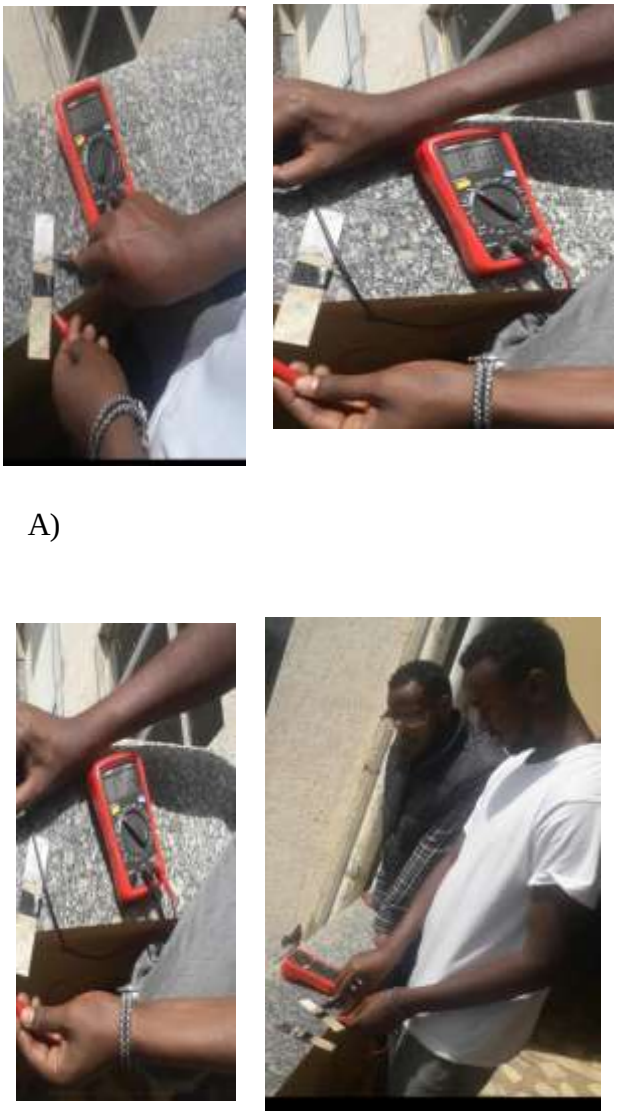

A) B)

C) D)

Figure 33:.(A) shows the voltagSe reading for KI electrolyte test and (B) shows the current reading and the letter (C) shows resistance test for starch gel electrolyte D) The resistance for KI test

4 .2.1 The basic difference in performance starch gel and potassium iodide electrolyte

In the liquid electrolyte test, the current generated was two times greater than the current produced by cells with gel electrolytes because, in a liquid medium, the ionic conductivity and capacity of the electrolyte to interact with TiO_2 particles were greater. The high current value, when first dropped by the electrolyte, decreased and only

lasted for 44 min. Thus, the current stability was not as good as that when using gel electrolytes. The oxidation levels are also high, which can reduce the cell quality. In addition, the longer temperature measurement of cells increases the heat that causes the rapid evaporation of electrolytes. This means that the iodine level decreased, so the ionic conductivity decreased. However, the current produced by the extract DSSC sandwich, which is 250 μA, is the maximum which produces no more than 250 μA for liquid electrolytes and only 35 μA for starch gel electrolyte

4.3 The new model (Sandwich Structure)

4.3.1 Dye Sensitized Solar Cell, candle smoke and Tio2 paste

Mesoporous photoanodes cannot uniformly cover the surface of the entire microscopic substrate slide glass; thus, in DSSCs, the electrolyte contacts the microscopic substrate slide glass. Furthermore, at this point, which is the microscopic glass-electrolyte boundary, charge recombination limits electron collection and, in turn, affects photo conversion efficiency (PCE).

The alteration of this boundary enhances the performance of DSSCs by overturning the recombination of electrons from the microscopic substrate slide to the electrolyte. This can be achieved by adding a compact metal oxide blocking layer onto a microscopic slide, which limits the back electron transport from the microscopic substrate slide to the electrolyte. For this study, titanium was hand-coated onto a microscopic slide using a stirrer, which was used as a blocking layer for both the CE and photoanode. Figure 29 shows the DSSCs assembled for the current study.

4.3.2 The mechanism of photo-electric conversion of the chlorophyll-sensitized DSSC

Upon illumination of the cell, the molecules of chlorophyll dye (D) are excited (D^*) after absorbing photons (hv) [eq 1].

$$hv + D \rightarrow D^* \text{ ---------- eq 1}$$

The excited chlorophyll molecules (D^*) inject electrons into the TiO_2 semiconductor conduction band, and the excited dye is then oxidized or ionized (D^+) [eq 2].

$$D^* + TiO_2 \rightarrow D^+ + e^-_{cb}(TiO_2) \text{ ----------eq 2}$$

The oxidized chlorophyll dye molecules (D^+) accept electrons from the iodide ion (I^-) in the electrolyte when the I- ions are released to the oxidized molecules and are in turn oxidized to triiodide ions (I_3^-) [eq 3].

$$2D + 3I^- \rightarrow I_3^- + 2D \text{ ----------eq (3)}$$

The electrons in the TiO_2 conduction band flow out of the device through the load to reach the

counter electrode and reduce the triiodide ions [Eq. 4].

$$I_3^- + 2e^- \rightarrow 3I^- \text{ ----------eq 4}$$

The iodide ion was restored, the electron circuit was completed, and the entire system returned to its original state to start a new cycle. These processes continue as long as the cell receives light, and the resulting current is continuously produced in the external circuit. When light shines on the cell, the observed voltage is given by the energy difference between the Fermi level of the photoanode and redox potential of the electrolyte.

CHAPTER FIVE

5. Conclusion and Recommendations

5.1. Conclusion

In this study, thin films were fabricated (constructed) to assemble chlorophyll-sensitized solar cells using candle smoke as a cathode and Tio2 coted conductive microscopic glass as the anode, and potassium iodide and starch gel(bula) as electrolytes, forming a Sandwich Structure. Chlorophyll dye was successfully extracted from *azardinchita (*neem) leaves, which was confirmed by infrared spectroscopy and XRD diffraction analysis. External current flow occurs when light shines on the anode. The photovoltaic performance of the assembled DSSC was measured using a multimeter under direct sunlight illumination. Furthermore, the assembled cell efficiency was determined by plotting an I-V curve. The current and voltage values for the cell were 33.33 µA /mm$^{2\ for}$ the potassium iodide electrolyte test and 4.66 µA/mm^2 for the starch gel electrolyte as the short-circuit case and 540 kVand180kV for the potassium iodide and starch gel, respectively.

According to our research, the lifetime of the DSSC with liquid electrolyte was approximately one week to ten days; however, by replacing the liquid electrolyte with the gel electrolyte, the lifetime of the DSSC increases by a factor of ten times. Therefore, DSSCs using gel electrolytes exhibit better lifetime performance than those assembled with classical liquid electrolytes. Based on the results obtained, the coupling of candle smoke and the use of a naturally synthesized dye can enhance the photocatalytic and photoluminescence properties of titanium. In addition, there is great potential for incorporating candle smoke (carbon) for use as a counter electrode in dye-sensitized solar cells.

5.2. Recommendations

The following comprehensive recommendations are proposed based on the findings of this study.

1) More focus should be placed on natural-based chlorophyll-synthesized solar cells to decrease the economic cost and upscale from lab-based to commercial products.
2) Experimental and Computational work should be conducted on a hand-to-hand basis.
3) Intensive research should be conducted on indigenous plant species grown in Ethiopia for their application in solar cells.

4) For further work, the university should encourage and focus on recent technological areas of nanotechnology and dye-synthesized solar cells.
5) For the prototype, further work to be done at the university should include the necessary chemicals and equipment.

REFERENCES

1. Kroposki B, Margolis R, Ton D. Harnessing the sun. *IEEE power and energy magazines*. 2009;7(3): 22-33.
2. Fleming RJ. Source of Earth's Thermal Blanket and Energy Balance. In: *The Rise and Fall of the Carbon Dioxide Theory of Climate Change 2020* (pp. 61-67). *Springer, Cham*.
3. Grätzel M. Dye-sensitized solar cells. *Journal of Photochemistry and Photobiology C: Photochemistry Reviews*. 2003;4(2): 145-153.
4. McConnell I, Li G, Brudvig GW. Energy conversion in natural and artificial photosynthesis. *Chemistry & biology*. 2010;17(5): 434-447.
5. Lamba R, Shirage PM. *Fabrication of TiO_2 based dye-sensitized solar cells with natural dyes* (Doctoral dissertation, Discipline of Physics, IIT Institute).
6. Matos A, Mendes F, Valente A, Morais T, Tomaz AI, Zinck P, Garcia MH, Bicho MB, Marques F. Ruthenium-based anticancer compounds: insights into their cellular targeting and mechanism of action. *Ruthenium Complexes*. 2018: 164.
7. Tributsch H. Reaction of excited chlorophyll molecules at the electrodes and photosynthesis. *Photochemistry and Photobiology*. 1972;16(4): 261-269.
8. Taya SA, El-Agez TM, El-Ghamri HS, Abdel-Latif MS. Dye-sensitized solar cells using fresh and dried natural dyes. *International Journal of Materials Science and Applications*. 2013;2(2): 37-42.

9. El-Agez TM, El Tayyan AA, Al-Kahlout A, Taya SA, Abdel-Latif MS. Dye-sensitized solar cells based on ZnO and natural dyes. *International Journal of Materials and Chemistry*. 2012;2(3): 105-110.
10. Abdel-Latif MS, El-Agez TM, Taya SA, Batniji AY, El-Ghamri HS. Plant seed-based dye-sensitized solar cells. *Materials Science and Applications*. 2013;4(09): 516.
11. Wongcharee K, Meeyoo V, Chavadej S. Dye-sensitized solar cell using natural dyes extracted from rosella and blue pea flowers. *Solar Energy Materials and Solar Cells*. 2007;91(7): 566-571.
12. Roy MS, Balraju P, Kumar M, Sharma GD. Dye-sensitized solar cells based on Rose28 Bengal dye and nanocrystalline TiO_2. *Solar Energy Materials and Solar Cells*. 2008;92(8): 909-913.
13. Wang ZS, Cui Y, Hara K, Dan-oh Y, Kasada C, Shinpo A. A high light-harvesting efficiency coumarin dye for stable dye-sensitized solar cells. *Advanced Materials*. 2007;19(8): 1138-1141.
14. Etula J. Comparison of three Finnish berries as sensitizers in a dye-sensitized solar cell. *European Journal of Young Scientists and Engineers*. 2012;1: 5-
23.
15. Ahmadian R. Estimating the impact of dye concentration on the photoelectrochemical performance of anthocyanin-sensitized solar cells: A power-law model. *Journal of Photonics for Energy*. 2011;1(1): 011123.
16. Hernandez-Martinez AR, Estevez M, Vargas S, Quintanilla F, Rodríguez R. Natural pigment-based dye-sensitized solar cells. *Journal of Applied Research and Technology*. 2012;10(1): 38-47.
17. Nagai H, Sato M. Heat treatment in molecular precursor method for fabricating

metal oxide thin films. Heat Treatment—Conventional and Novel

Applications; Czerwinski, F., Ed. 2012: 297-322.
18. Daniel LS. Electrical conductivities, Plasmonic properties and vis-responsive activities of Ag-Nanoparticles/ Titania composite thin films fabricated using Molecular Precursor Method (MPM). Dissertation 2014. Kogakuin University, Japan.
19. Sharma K, Sharma V, Sharma SS. Dye-sensitized solar cells: Fundamentals and Current Status. *Nanoscale research letters*. 2018;13(1): 381. Available from: https://doi.org/10.1186/s11671-018-2760-6.
20. University of California, Los Angeles. Extraction of chlorophyll from fresh spinach and investigation of chlorophyll photochemistry
21. Shalini S, Balasundaraprabhu R, Kumar TS, Prabavathy N, Senthilarasu S, Prasanna S. Status and outlook of sensitizers/dyes used in dye sensitized solar cells (DSSC): a review. *Int. J. Energy Res*. 2016;40(10):1303-1320. Available from: doi: 10.1002/er.3538.
22. Martineau D. Dye Solar Cells for Real: The Assembly Guide for Making Your Own Solar Cells. Solaronix, REV. 2012;3: 12.
23. Riaz R, Ali M, Maiyalagan T, Arbab AA, Anjuk AS, Lee S, Ko MJ, Jeong SH. Activated charcoal and reduced graphene sheet composite structure for highly

electrocatalytically active counter electrode material and water treatment. *International Journal of Hydrogen Energy*. 2019: 1-13. Available from: doi.org/10.1016/j.ijhydene.2019.06.138.

24 Daniel LS, Nagai H, Yoshida N, Sato M. Photocatalytic Activity of Vis Responsive Ag-Nanoparticles/TiO_2 Composite Thin Films Fabricated by Molecular Precursor Method (MPM). *Catalysts*. 2013;3(3): 625-645.

Available from: doi: 10.3390/catal3030625

25 Ghann W, Kang H, Sheikh T, Yadav S, Chavez-Gil T, Nesbitt F, Uddin J. Fabrication, optimization, and characterization of natural dye-sensitized solar cells *Rep*. 2017;7: 41470. Available from: doi: 10.1038/srep41470.

26 Arbab AA, Sun KC, Sahito IA, Memon AA, Choi YS, Jeong SH. Fabrication of textile fabric counter electrode using activated charcoal doped multi-walled carbon nanotube hybrids for dye-sensitized solar cells. *J. Mater. Chem. A*. 2016;4(4): 1495-1505. Available from: doi: 10.1039/c5ta08858e.

27 Arbab AA, Sun KC, Sahito IA, Qadir MB, Choi YS, Jeong SH. Novel activated-charcoal-doped multiwalled carbon nanotube hybrid for quasi-solid-state dye-sensitized solar cells outperforming Pt electrodes. *ACS App. Mater. Interfaces*. 2016;8(11): 7471-7482.

28 Pramono SH, Maulana E, Prayogo AF, Djatmika R. Characterization of dye-sensitized solar cells (DSSC) based on chlorophyll dyes. *International Journal of Applied Engineering Research*. 2015;10(1): 193-205.

29 Memon AA, Arbab AA, Sahito IA, Sun KC, Mengal N, Jeong SH. Synthesis of highly photocatalytic and electrocatalytic active textile-structured carbon electrodes and their application in DSSCs. *Solar Energy*. 2017;150: 521-531. Available from: http://dx.doi.org/10.1016/j.solener.2017.04.052.

30 Selvaraj P, Roy A, Ullah H, Sujatha Devi P, Tahir AA, Mallick TK, Sundaram S. Soft-template synthesis of high surface area mesoporous titanium dioxide for dye-sensitized solar cells. *Int. J. Energy Res*. 2019;43(1): 523-534. Available from: doi: 10.1002/er.4288.

31 Alhamed M, Issa AS, Doubal AW. Study the properties of natural dyes as photosensitizers for dye-sensitized solar cells (DSSC). Journal of electron Devices. 2012;16(11): 1370-1383.

32 Wang XF, Kitao O. Natural chlorophyll-related porphyrins and chlorins for dye-sensitized solar cells. *Molecules*. 2012;17(4): 4484-4497.

33 Syafinar R, Gomesh N, Irwanto M, Fareq M, Irwan YM. Chlorophyll pigments are nature-based dyes used in dye-sensitized solar cells (DSSC). *Energy Procedia*. 2015;79: 896-902. Available from: doi: 10.1016/j.egypro.2015.11.584.

34 Sun KC, Memon AA, Arbab AA, Sahito IA, Kim MS, Yeo SY, Choi YO, Kim YS, Jeong SH. An electrocatalytic porous nanocomposite of graphite nanoplatelets anchored with exfoliated activated carbon

filler was used as a counter electrode for dye-sensitized solar cells. Solar Energy. 2018;167: 95-101.

35 Calogero G, Citro I, Di Marco G, Minicante SA, Morabito M, Genovese G. Brown seaweed pigment as a dye source for photoelectrochemical solar cells.

Spectrochimica Acta Part A: Molecular and Biomolecular Spectroscopy. 2014;117: 702-706.

36 Godibo DJ, Anshebo ST, Anshebo TY. Dye-sensitized solar cells using natural pigments from five plants and a quasi-solid-state electrolyte. Journal of the Brazilian Chemical Society. 2015;26(1): 92-101.

37 Arof AK, Ping TL. Chlorophyll as a photosensitizer in Dye-Sensitized Solar Cells. Chlorophyll. 2017: 105.

38 Eli D, Musa GP, Ezra D. Chlorophyll and betalain as light-harvesting pigments for nanostructured TiO_2 based dye-sensitized solar cells. Journal of Energy and Natural Resources. 2016;5(5): 53-58.

39 Shah S, Buraidah MH, Teo LP, Careem MA, Arof AK. Dye-sensitized solar cells with sequentially deposited anthocyanin and chlorophyll dyes as sensitizers. Optical and Quantum Electronics. 2016;48(3): 219.

40 Shanmugam V, Manoharan S, Sharafali A, Anandan S, Murugan R. Green grasses as light harvesters in dye-sensitized solar cells. Spectrochimica Acta Part A: Molecular and Biomolecular Spectroscopy. 2015;135: 947-952.

41 Atkins P, Overton T, Rourke J, Weller M, Armstrong F, Hagerman M. Shriver

and Atkins' Inorganic Chemistry. 5th ed. New York: W. H. Freeman and Company (2010)

42 Robinson JW, Frame EMS, Frame II GM. Undergraduate instrumental

analysis. 7th ed. 2014.

43 Skoog DA, Holler FJ, Crouch SR. Principles of Instrumental Analysis. 6th ed.

Canada: David Harris (2007)

44 Harris DC. Quantitative chemical analysis. 8th ed. United States of America (USA) Clancy Marshall; 2010.

45 Edaq. Echem Manual. 1999.

46 Ohno T, Sarukawa K, Tokieda K, Matsumura M. Morphology of a TiO_2

The photocatalyst (Degussa, P-25) consisted of anatase and rutile crystalline phases. *J Catalysis.* 2001; 203: 82-86.

47 Thiruvenkatachari, R, Vigneswaran, S, Moon, IS. Review of the UV/TiO_2 photocatalytic oxidation process. *Korean J. Chem. Eng*. 2008; 25(1): 64-72.

48 .Ohtani B, Prieto-Mahaney OO, Li D, Abe R. What is Degussa (Evonik) P25? Crystalline composition analysis, reconstruction of isolated pure particles, and photocatalytic activity test.

49 .Hurum DC, Agrios AG, Gray KA et al.. Explaining the Enhanced Photocatalytic Activity of Degussa P25 Mixed-Phase TiO_2 Using EPR. *J. Phys. Chem. B*. 2003; 107: 4545-4549.

50 ..Raihana M. Performance analysis of Graphite and Multi Wall Carbon Nanotube based Counter Electrodes in Dye Sensitized Solar Cells, *University of Dhaka*. M. Sc. Thesis, 2016.

51 .Kalipi M. Performance enhancement of Ag-NP/TiO_2 using Chlorophyll as dye sensitizer, *University of Namibia*. M. Sc. Thesis, 2019.

52.A.R. Jha, P. . (2010). *Solar Cell Technology and applications*. (L. Taylor and Francis Group

(ed.)). 2010 by the Taylor and Francis Group, LLC.

53.Nurrida, C Mulyana, T Susilawati, A Bahtiar and A Aprilia, L. S. (2017). Calculation of DSSC parameters based on ZnO nanorod / TiO_2 mesoporous photoanode. *ICGRER*, 75, 2–8.

54. Adedokun, O., Titilope, K., & Awodugba, A. O. (2016). Review on Natural Dye-Sensitized

Solar Cells (DSSCs). *International Journal of Engineering Technologies*, 2, 34–41.

55.Ahliha, A. H., Nurosyid, F., & Supriyanto, A. (2017). Chemical Bonds Effect of Amaranthus Hybridus L. and Dracaena Angustifolia on TiO_2 as a photosensitizer for dye-sensitized solar cells (DSSC). *AIP Conference Proceedings*, 1868, 1–6.

56.Ahmad, S., Saeidi, M., Rahmanian, R. (2015). Photoelectric characterization of fabricated dye-sensitized solar cells using dye extracted from red Siahkooti fruit as a natural sensitizer. Spectrochimica Acta Part A: Molecular and Biomolecular Spectroscopy, 142, 226–231.

57.Al, M. M., Ahmed, N. M., & Hasanein, A. A. (2020). Molecular modeling and photovoltaic applications of porphyrin-based dyes. Journal of Saudi Chemical Society, 24(January), 303–320.

58.Amalathas, A. P. (2019). Nanostructures for light trapping in thin-film solar cells. 10, 1–

18.

58.Antonio Luque, & Hegedus Steven. (2003). Handbook of Photovoltaic Science and

Engineering.

59.Attanayake, I., De Silva, C., Premachandra, B.A.J. K., De Alwis A. A. P., Senadheera G.K.R. (2013). Dye-sensitized solar cells: Using over 100 natural dyes as sensitizers.
1–16.

60.Bagher, A. M., Mahmoud, M., Vahid, A., Mohsen, M. (2015). Types of Solar Cells and

Application. 3, 94–113.

61.Barbose Galen, Bolinger Mark, W. R. and M. D. (2017). Climate and air quality benefits of wind and solar power in the United States. *Nature Energy*, 2, 2–28.

62.Berthomieu, C. and Hienerwadel, R. (2009). Fourier-transform infrared (FTIR) spectroscopy. *Photosynthesis Research*, 101, 157–170.

63. Bose, S., Soni, V., Genwa, K.R. (2015). Recent Advances and Future Prospects for Dye

Sensitized Solar Cells: A Review. *International Journal of Scientific and Research Publications*, 5, 1–9.

64.Calogero, G., Yum, J., Sinopoli, A., Di, G., & Gra, M. (2012). Anthocyanins and betalains are light-harvesting pigments used in DSSCs. *Solar Energy*, 86, 1563–1575.

65.Cari, Supriyanto, A., Fadli, U. M., & Prasada, A. B. (2016). Fabrication and Characterization of Sansevieria trifasciata, Pandanus amaryllifolius and Cassia angustifolia as

Photosensitizers for dye-sensitized solar cells. Journal of Physics: Conference Series 710, 2–8.

66.Cavallo, C., Di Pascasio, F., Latini, A., Bonomo, M., & Dini, D. (2017). Nanostructured

Semiconductor materials for Dye-Sensitized Solar Cells. *Journal of Nanomaterials*, 2017, 1–32.

67. Chandiran, A. K., Abdi-jalebi, M., Nazeeruddin, M. K., Gra, M. (2014). Analysis of the Electron Transfer Properties of ZnO and TiO_2 Photoanodes for Dye-Sensitized Solar Cells. *Acsnano*, 8(February), 2261–2268.

68.Cheknane, A., Hilal, H. S. (2008). Equivalent circuit approach for organic solar cell modelling. *Microelectronics Journal*, 39, 1173–1180.

69.Cherepy, N. J., Smestad, G. P., Gra, M., & Zhang, J. Z. (1997). Ultrafast Electron Injection

Implications for a photoelectrochemical cell utilizing an anthocyanin-dye-sensitized TiO2 nanocrystalline electrode. J. Phys. Chem. B, 101(September), 9342–9351.

70.Chien, C., & Hsu, B. (2013). Optimization of dye-sensitized solar cells with anthocyanin as a photosensitizer. Solar Energy, 98, 203–211.

71.Concina, I., & Vomiero, A. (2014). Metal Oxide Semiconductors for Dye- and Quantum-Dot-

Sensitized Solar Cells. Materials Views 2, 1–31.

72. Conibeer, Gavin & Willoughby, A. (2014). Development of solar cell materials JohnWiley & Sons, Ltd., registered C.

73.Diau, E. W.-G. (2017). Next-generation solar cells and solar energy *conversion ACS*

Energy Letters, 2(January), 334−335.

74 .Du, Y., Wang, X., Lian, D., Liu, Y., Zhang, L., Xu, S., & Cao, S. (2020). Dendritic PAMAM polymers for strong perovskite intergranular interactions enhance the power conversion efficiency and stability of perovskite solar cells. Electrochimica Acta, 349, 1–12.

75. Dumbravă, A., Enache, I., and Oprea, C. I., Georgescu, A., & Gîrţu, M. A. (2012). Toward more efficient utilization of betalains as pigments for dye-sensitized solar cells. *Digest Journal of Nanomaterials and Biostructures*, 7, 339–351.

76. Ebrahim, K. (2011). Dye Sensitized Solar Cells - Working Principles, Challenges and

Opportunities. Solar Cells: Dye-Sensitized Devices, 172–204.

77. Frost, J. M. (2015). Multiscale physics of Photovoltaics. From Atoms to Solar Cells, UK.

78 .Ghann, W., Kang, H., Sheikh, T., Yadav, S., Chavez-gil, T., Nesbitt, F. (2017). Fabrication

Optimization and characterization of natural dye-sensitized solar cells *Scientific Reports*, 7, 1–12.

79. Ghernaout, D., Boudjemline, A., Elboughdiri, N. (2020*). Electrochemical Engineering in the Core of the Dye-Sensitized Solar Cells (DSSCs). Open Access Library Journal, 7, 1–12.*

80. Godibo, D. J., Tadesse, S., Anshebo, T. Y. (2014). Dye-sensitized solar cells were fabricated using natural pigments from five plants and a quasi-solid-state electrolyte.

81. Gong, J., Sumathy, K., Qiao, Q., Zhou, Z. (2017). Review on dye-sensitized solar cells (DSSCs): Advanced techniques and research trends. *Renewable Sustainable Energy Reviews*, 68, 234–246.

82. Wahidah et al. (2018). A natural dye-sensitized from prepare (Bitter Gourd) leaf extracts for DSSC. Al-Kimia, 1–9.

83. Zulkifili, A. N. B., Kento, T., Daiki, M., & Fujiki, A. (2015). The Basic Research on the Dye-Sensitized Solar Cells (DSSC). Journal of Clean Energy Technologies, 3, 382–387.

84 . Rossi, M., Matteocci, F., A, D. C., Forni, C. (2017). Chlorophylls and xanthophylls of crop plants are dyes used in dye-sensitized solar cells (DSSC). *Journal of Plant Science and Phytopathology*, 1(October), 087–094.

85. Sanjay, P., Deepa, K., Madhavan, J., Senthil, S. (2018). Fabrication of DSSC with Nanostructured TiO 2 Photoanode and Natural Dye Sensitizer extracted from fruits of Phyllanthus reticulatus. IJSRST, 4(5), 437–443.

86 Sarker, S., Woo, H., Lee, K., Jin, Y., Ju, H., & Min, D. (2015). Exact analytical analysis of current density – voltage curves of dye-sensitized solar cells. 115, 390–395.

87 Leach, G. & Merkle, R. C. (1991). Computational nanotechnology. *Nanotechnology*, 2(February), 134–141.

88 Lee, J., & Yang, M. (2011). Progress in light harvesting and charge injection in dye-sensitized solar cells. *Materials Science & Engineering*, June, 1142– 1160